Deliverable 4.1

Recommendations for weakly coupled physical-biogeochemical data assimilation

Deliverable Contributors:	Name	Organisation	Role / Title
Deliverable Leader	Nerger, L.	AWI	Task 4.1 leader
Contributing Author(s)	Brasseur, P.	CNRS	Contributor
	Popov M.	UGA	Contributor
	Skakala J.	PML	Contributor
	Teruzzi A.	OGS	Contributor
	Cossarini G.	OGS	Contributor
Reviewer(s)	Bertino, L.	NERSC	WP4 leader
Final review and approval	Skákala, J.	PML	Project Coordinator

Project	SEAMLESS No 101004032	Deliverable	D4.1
Dissemination	Public	Type	Report
Date	21 July 2023	Version	4.0

Document History:

Release	Date	Reason for Change	Status	Distribution
1.0	31-07-2022	Initial document, reviewed		Internal
2.0	31-08-2022	Revised document	It misses AWI's contribution on the Baltic sea	Internal/EC
3.0	10-11-2022	Revised with updated inputs from partners except for BAL	Contribution on BAL region still missing	Internal
4.0	21-07-2023	Final version with inputs from all partners	Submitted	public

To cite this document

Nerger. *et al.* (2023). D4.1 Recommendations for weakly coupled physical-biogeochemical data assimilation. Deliverable report of project H2020 SEAMLESS (grant 101004032).

Project	SEAMLESS No 101004032	Deliverable	D4.1
Dissemination	Public	Type	Report
Date	21 July 2023	Version	4.0

TABLE OF CONTENTS

Project	SEAMLESS No 101004032	Deliverable	D4.1
Dissemination	Public	Type	Report
Date	21 July 2023	Version	4.0

1. Scope

The scope of this document is (i) to report on the developments of weakly coupled ensemble assimilation methods and assimilation experiments performed in WP4 (Task 4.1), and (ii) to provide methodological recommendations to perform weakly coupled physical-biogeochemical data assimilation in the CMEMS MFC 3D domains.

Each partner in support of a particular MFC (AWI for BAL; OGS for MED; PML for NWS; UGA for GLO and IBI) implemented assimilation experiments in 1D or 3D setups as compliant as possible with the one used by the CMEMS systems in operation today, in order to facilitate the transfer of methods and results towards MFCs and to draw recommendations applicable to each MFC. This deliverable is building upon deliverable D3.2 (based on 1D experiments) and deliverable D3.4 (based on 3D experiments), addressing the prospects of coupled physical-biogeochemical data assimilation as deemed relevant for each MFC.

2. Introduction

The current operational bio-modelling systems *do not draw the maximum benefit* from assimilation of physical data, some even suffer deterioration of the biogeochemistry after assimilation of physical data.

The overall objective of WP4 is to remove a blocking point for the mutual consistency of physical and BGC assimilation practices in CMEMS.

Our hypotheses are the following:

- *Ensemble methods developed in WP3 can increase the reciprocal controllability of physical and biogeochemical states of the coupled models.*

- *Other methods can mitigate deteriorations.*

This document is structured as follow: In section 3 the choices for the experiment designs used in the different MFC domains are described. The results of the assimilation experiments obtained in Task 4.1 in the different MFC regions are reported in section 4. Ensemble diagnostics are described in terms of (i) observed state variables, (ii) non-observed state variables and (iii) relevant SEAMLESS indicators (leveraging from the conclusions of Tasks 3.2 and 3.3). In section 5, the results obtained for indicators are discussed with a focus on phenology, POC flux, primary production, grazing efficiency and PFTs (pH and O_2 being of lesser relevance following the conclusions of Task 3.2). Finally in section 6, we outline the methodology to assess observability/controllability/identifiability (OCI) metrics and provide guidelines for its application to assess BGC products in the 5 MFCs and their integration in the CMEMS catalogue.

3. Experimental Design Choices

In this section, the choices for the assimilation experiments are described. This builds on the assimilation methods developed and tested by the partners in Task 3.3 (see Deliverable D3.4), and the assimilation gaps that SEAMLESS aims to bridge with respect to the methods in operation today in the different centres. A schematic illustration of the transition to ensemble-based assimilation methods as achieved by SEAMLESS for BGC monitoring and forecasting in the different MFCs is given in Table 3.1.

Partner	CMEMS MFC	1D Station	DA used in CMEMS	Target WP4 Method
AWI	BAL	Arkona	LESTKF (fixed basis)	LESTKF dynamic ensemble
UGA	GLO / IBI (N. Atl.)	PAP	SEEK (fixed basis)	Stochastic ensemble
OGS	MED	Floats (eastern and western Med)	3DVAR	Hybrid Ens.-3DVAR
PML	NWS	L4	3DVAR	Hybrid Ens.-3DVAR

Table 3.1 Overview of model configurations and data assimilation methods used in D4.1

3.1 Experimental design for the BAL MFC domain

For the weakly coupled data assimilation in the Baltic Sea in SEAMLESS we base on the developments of WP3. Thus, we use a system in which NEMO-ERGOM is coupled online with PDAF (Nerger et al., 2013). This is performed by augmenting the NEMO-ERGOM source code with data assimilation functionality provided by PDAF. A fully dynamic ensemble is used to estimate the covariance matrix at the time of each analysis step. The initial ensemble for the physical variables is generated by creating ensemble perturbations using second-order exact sampling using singular vectors (covariance matrix information) from snapshots of a free running model. An ensemble of 30 members is used. The ensemble spread for the biogeochemical model fields is zero at the initial time. We perturb 15 process parameters of ERGOM and then run the ensemble for one month, which generates ensemble spread for the biogeochemical fields. This one-month spinup is also motivated by the fact that during January the number of satellite observations of chlorophyll is very low due to the cloud cover and hence the possibilities to apply data assimilation are very limited.

The data assimilation process is started on February 1, 2015 at the end of the 1-month spinup. Note that this is earlier than in Deliverable 3.4, where the assimilation was started by March 1. However, as discussed in Deliverable 3.4, the phytoplankton bloom at the validation station Arkona started already in February. Thus, while the amount of satellite chlorophyll observations in February is still very limited, it was useful to start the assimilation already at the onset of the bloom because the initial changes by the assimilation are smaller and hence the initial assimilation 'shock' is lower. The assimilation is performed daily until the end of May 2015 to cover the spring bloom in the Baltic Sea.

The satellite observations considered here are a level-3 multi-satellite product of sea surface temperature (SST) from CMEMS and level-3 multi-satellite data products of chlorophyll, also provided by CMEMS. For chlorophyll, there are two separate products for the North Sea and Baltic Sea and both are used here. The two products overlap in the transition zone between North Sea and Baltic Sea. To avoid using two products at the same location, the North Sea product is used in the Kattegat only north of 56.8°N, while the product for the Baltic Sea is used from 56.8°N southward.

To assess the effects of weekly coupled DA, four different experiments are performed:

- FREE: In this experiment the ensemble is run freely without assimilation.
- CHL-DA: In this experiment only the satellite chlorophyll data are assimilated.
- SST-DA: In this experiment only the satellite SST observations are assimilated.
- CHL+SST-DA: This experiment performed the combined assimilation of SST and chlorophyll observations.

In all cases the assimilation is performed with a weakly-coupled configuration. Thus, the physical SST observations only influence the physical variables of NEMO directly. Likewise, the chlorophyll observations are only used to directly update the ERGOM biogeochemical variables in the analysis step. The fields of the other model component are then only influenced by the model dynamics during the 24-hour forecast phase following the analysis update.

The SST observations only change the 3-dimensional temperature field in the analysis step. Including more physical variables led to unstable model dynamics with unrealistically high salinity and was abandoned. For ERGOM, all variables except Alkalinity, DIC and dissolved organic matter represented as nitrogen (LDON) are included in the state vector and updated when chlorophyll observations are assimilated. Including, in particular, alkalinity in the state vector resulted in negative alkalinity during the model integrations, while the dynamic reaction of alkalinity was stable.

3.2 Experimental design for the GLO and IBI MFC domains

This section describes the design of the weakly coupled assimilation experiments implemented by **IGE/UGA** to assess how the 4D stochastic ensemble method developed in WP3 can be used to assimilate physical and biogeochemical data more consistently into the coupled NEMO-PISCES model, in the context of the GLO and IBI systems.

In the CMEMS Global BGC forecasting/analysis system in operation today, the PISCES model equations are forced – or "weakly coupled" – with physical fields that are constrained with assimilated temperature, salinity and sea level anomalies. Yet, while physical data assimilation substantially improves the physical fields, BGC models forced by such reanalyses are usually degraded as a result of spurious biological adjustments induced by imperfect physics (Gasparin *et al*., 2021). This problem was first highlighted by Berline *et al*. (2006), who attributed the main cause to intermittent re-initialization of the sequential assimilation scheme. The 4D space-time inverse approach developed in WP3 has been precisely designed to avoid such intermittent reinitialization, still allowing independent ("weakly coupled") or joint ("strongly coupled") assimilation of physical and biogeochemical data.

Furthermore, there is no need to introduce additional constraints since, by design, dynamical consistency of the ensemble members should be preserved.

The weakly coupled experiments carried out by IGE as part of Task 4.1a combine the assimilation of CMEMS L3 along-track satellite altimetric data (SSH) and ocean colour (OC) data in the regional configuration intersecting GLO and IBI domains around PAP station (48°50'N, 16°30'W) following the WP3 approach. The algorithm is built on a separation between the prior ensemble generation which relies on the full model complexity, and the posterior pdf computation which makes the inverse problem simpler and avoids re-initialization and time-integration of the full coupled model while still allowing probabilistic forecasts (see D3.4). The design of 4D experiments illustrated by Figure 3.1 includes the following steps:

- *Prior coupled physical-biogeochemical model ensemble*. We use the prior 40-member ensemble already generated during year 2019 for WP3 developments (see D3.4), assuming uncertainty sources originating from (i) critical biogeochemical model parameters of the PISCES stochastic formulation, (ii) sub-grid scale effects associated to ¼°, eddy-permitting horizontal resolution, and (iii) location uncertainties of mesoscale structures and associated advective/diffusive fluxes, accounting for coupled physical/biogeochemical effects.

- *Space-time data selection and preparation*. The prior model ensemble data set is extracted during the period March 15th, 2019, through June 15th, 2019. During this 3-month period, the L3 CMEMS products include along-track data from 6 altimetric satellites (Sentinel-3A, Sentinel-3B, Jason-3, Cryosat-2, AltiKA, HY-2A) and daily ocean colour data at 4 km from 4 satellites (MODIS, VIIRS and Sentinel-3A/B sensors). The spread of the physical prior ensemble is inflated before anamorphic transformations using an adjustable multiplicative factor. In addition, the ensemble members SSH is adjusted to ensure statistical consistency with the altimetric data set.

- *First observational update of the prior distribution by altimetric data*. Altimetric observations from 4 satellites (Sentinel-3A/B, Jason-3, HY-2A) are first assimilated during the period (between March 15th and May 15th) using the LETKF analysis scheme implemented in 4D, accounting for space-time correlations between state variables. A space-time localization scheme is applied with a cutting length/time of 100 km/30 days and a correlation length/time of 40 km/10 days. An additive observation error of 3 cm (std) is assumed for altimetric data. The period from May 15th to June 15th is considered as experimental period to assess the predictive skill of the *probabilistic forecast*. The two non-assimilated altimeter data sets (AltiKA, Cryosat-2) are used as independent verification data to estimate the uncertainty of the distributions.

- *Second observational update of the distribution by ocean colour data*. In a second stage, OC L3 data are assimilated between March 15th and May 15th in *hindcast mode* using the same 4D analysis scheme applied to the distribution previously conditioned by altimetric data assuming a 30 % multiplicative observation error. The period from May 15th to June 15th is again considered as experimental period to assess the skill of the probabilistic forecast.

In addition to the physical NEMO state variables, 17 PISCES state variables are updated by the SLA and OC data assimilation scheme (7 PISCES variables of lesser importance are excluded from the estimation state vector to save CPU resources). This two-step update of the prior distribution mimics the weakly coupled assimilation concept as defined in SEAMLESS ("independent assimilation into

physical and BGC models, each compartment assimilating observations of its own kind") as well as the practical functioning of most modelling chains operated in CMEMS. The main goal (and interest) of WP4 will be to compare weakly coupled to strongly coupled assimilation (i.e., "joint update of physical and BGC state variables, exploiting error covariances between observations of different types") that will be explored in Task 4.2 by updating the physical and BGC ensemble variables with altimetric and ocean colour data assimilated simultaneously.

A particularity of the 4D algorithm implemented in these experiments is the substitution of the mechanistic model classically used for the prediction step of the ensemble Kalman filter by a statistical model built from the prior ensemble simulation, and the combination with anamorphic transformations to perform the inversion in a Gaussian space. This makes the implementation of a smoother (joint use of past and future observation) easier, thus avoiding the neglection of half of the observations to produce the current analysis. In this context, the "weakly coupled" algorithm described above means that the statistical model is used to flow information from physics to biology, but not the other way around. The fact that the method works as a smoother implies that past and future physical observations can indirectly influence the current biological state through the statistical model.
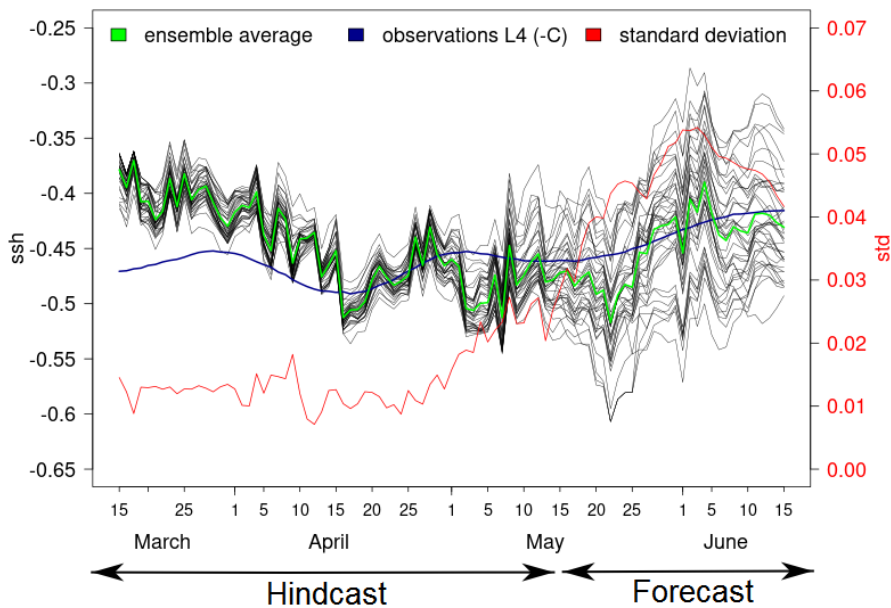

Figure 3.1: *Experimental design of weakly/strongly NEMO-PISCES coupled assimilation experiments, illustrated by the time series of SSH ensemble members at PAP station. Altimetric data from 4 satellites and ocean colour L3 products are assimilated daily during the hindcast period (from March 15th to May 15th, 2019). Observations available during the forecast period (from May 16th to June 15th, 2019) are used for verification.*

Nevertheless, in view of the nonlinear nature of the statistical model operator and the necessary approximations in the processing chain (anamorphic transformations, localization, ensemble inflation), the "weakly coupled" and the "strongly coupled" algorithms are likely to produce different results. This will be further investigated in Task 4.2.

3.3 Experimental design for the NWS MFC domain

The current **NWS** system is based on 3D-variational assimilation using the NEMOVAR software. The background covariance matrices are supplied as monthly climatologies, e. g. for biogeochemistry the climatological variances originate from a decadal EnKF reanalysis. The system uses spatially varying climatological horizontal length scales, whereas the vertical length scales are flow dependent and calculated based on the simulated mixed layer depth. The physical DA is performed by linearly transforming temperature, salinity, Sea Surface Height (SSH) and current velocity horizontal components into a set of independent variables and applying univariate assimilation to each of those. The biogeochemical variables are assimilated univariately, but after the assimilation, the system uses a balancing scheme to distribute the DA increments into some of the non-assimilated biogeochemical variables (e. g. spreading increments from total chlorophyll into all the components of the ERSEM Phytoplankton Functional Types, PFTs). The system is designed to assimilate, on a daily basis, Sea Surface Temperature (SST), temperature and salinity profiles, satellite ocean colour (OC)-derived total chlorophyll, PFT chlorophyll and optical data, and has also the capacity to assimilate glider data, such as chlorophyll and oxygen (Skakala et al, 2021). In its operational version it assimilates only SST, temperature and salinity profiles, and OC total chlorophyll.

The SEAMLESS developments address the background variances, as well as the length scales used by the system, i.e., these are now calculated from first principles using the ensemble, rather than provided externally by the climatological data. In WP3.3 we developed perturbations of the 6 most sensitive ERSEM parameters (determined by the 1D sensitivity analysis in WP3) and combined these with an atmospheric (ERA5) forcing ensemble and observation perturbations. These perturbations were incorporated into a 30-member physical-biogeochemical ensemble performing weakly coupled assimilation of physical data (satellite SST, temperature and salinity profiles) combined with satellite ocean colour-derived total chlorophyll. The assimilation is performed using a hybrid ensemble-3DVAR system, which was recently developed at the Met Office for global assimilation of physical data and adopted here for biogeochemical DA on the NWE Shelf. The model set-up uses two-way coupling between physics and biogeochemistry based on a spectra-resolving bio-optical module implemented into the model (Skakala et al, 2020, 2022).

3.4 Experimental design for the MED MFC domain

The current operational Marine Copernicus **MED** system consists of two distinct models: the ocean dynamic model (NEMO-WWIII), which includes the assimilation of Sea Level Anomaly (SLA) maps and temperature (T) and salinity (S) profiles, and the biogeochemical model (BFM, Salon et al., 2019), which features a variational assimilation scheme for satellite chlorophyll maps and chlorophyll and nitrate BGC-Argo profiles (Teruzzi et al., 2021). In the ocean dynamic system, daily SLA maps and profiles from Argo and XBT sensors are assimilated by means of a 3D variational assimilation scheme with a prescribed monthly and spatial varying background error covariance matrix (OceanVar; Dobricic and Pinardi, 2008 and Storto et al., 2015). In the biogeochemical system, data assimilation is performed with a 3D-variational approach with decomposition on the error covariance matrix in three operators that account for the vertical, horizontal and biogeochemical covariances. Satellite and BGC-Argo observations are weekly and daily assimilated, respectively.

The ocean dynamics and the biogeochemical models run separately, and the ocean dynamics model provides mean daily assimilated fields of physical variables (e.g., u, v, w, eddy diffusivity, T, and S) that force the transport and the evolution of biogeochemical variables. Thus, the current **MED** system consists of a weakly one-way physical assimilation that impacts biogeochemistry through the dynamical adjustment of the biogeochemistry. In addition, biogeochemistry is impacted directly by data assimilation of biogeochemical observations.

The objective of task 4.1 is to develop and test a balancing scheme based on the physical assimilation increments to be added in the prescribed background error covariance matrix for the direct update of nutrients (i.e., phosphate and nitrate) in the biogeochemical system. To test the update of biogeochemistry by the physical assimilation, the SEAMLESS 1D-prototype system has been applied using Argo and BGC-Argo data in two Mediterranean Sea locations (one in the western and one in the eastern). New developments include (a) a specific plugin in the SEAMLESS 1D-prototype featuring the prescribed error covariance between physical and nutrients fields and (b) the implementation of hybrid experiments that consist of an ensemble scheme (ESTKF) that assimilates T and S Argo profiles in the 1D system and a variational component based on prescribed covariances for the phosphate and nitrate updates. Differently from the current operational Marine Copernicus MED system, only Argo temperature and salinity are assimilated, and BGC-Argo observations are used for validation, while OC observations are not included in the experiments carried out in present deliverable.

The plugin is built as a python script that receives physical assimilation results (from an EnKF approach, but in principle other assimilation schemes can be used) as input and provides increments for phosphate and nitrates. In particular, the prescribed density/nutrient error covariance is computed from a statistical analysis of Argo and BGC-Argo floats in western and eastern Mediterranean basins (Feudale et al., 2021).

Given the specificity of the 3D MED system, the feasibility and transferability of the new assimilation scheme to the 3D MED system will be discussed based on the results of the 1D-system experiments.

4. Assimilation experiments

This section reports on assimilation experiments of WP4.1 for the different domains of the MFCs. The analysis assesses diagnostics on observed variables, diagnostics on non-observed variables, as well as diagnostics on derived quantities and SEAMLESS indicators.

4.1 Assimilation results in the BAL MFC domain

Diagnostics on observed variables

As observed variables, we consider chlorophyll and temperature. However, it depends on the experiment whether the variable is actually assimilated. In case that only SST data is assimilated in experiment SST_DA, the chlorophyll is unobserved, while temperature is unobserved if only chlorophyll data is assimilated in experiment CHL_DA. Both variables are only observed in the experiment CHL+SST_DA. We expect the RMSe of the assimilated variable to decrease significantly

and a hope for a slight decrease of the RMSe of the unassimilated chlorophyll when assimilating SST because a more realistic physical state should in principle benefit the biogeochemical state. We may also experience a deterioration of the RMSe if the assumptions of the data assimilation method are violated (biased model or observations, non-Gaussian distributed variables). Conversely, the assimilation of chlorophyll should not influence the physical state at all.

For the full Baltic Sea, Fig. 4.1.1 shows the root mean square error (RMSe) for surface chlorophyll and temperature over time. In the upper panel the RMSe for logarithmic concentrations of chlorophyll is shown. In January there are days without any satellite observations. On these dates no RMSe can be computed. The RMSe fluctuates strongly in February and March. This effect is mainly due to the varying coverage of the satellite data caused by data gaps in cloudy regions. The effect of the SST assimilation on the RMSe of chlorophyll is negligible. In contrast the two experiments that assimilate chlorophyll show a clear reduction of the RMSe of logarithmic concentrations from 0.40 in FREE and SST_DA to 0.29 in CHL_DA and 0.28 CHL+SST_DA is visible. Larger differences between the two assimilation experiments are visible during April, to the advantage of the coupled CHL+SST_DA run.
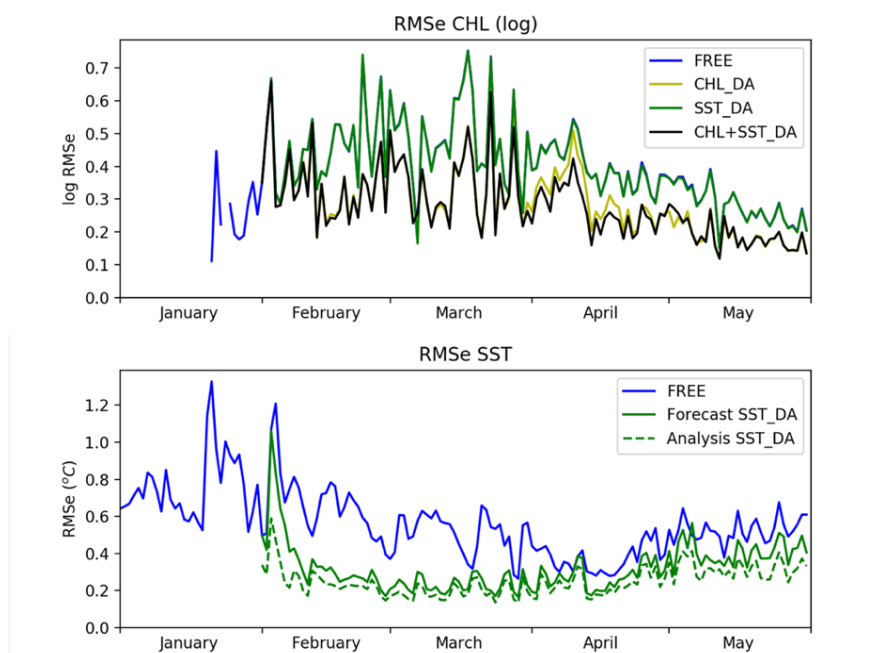

Fig. 4.1.1 *Root mean square error with regard to the satellite observations for the full Baltic Sea. Shown are the errors for the chlorophyll (top) and SST (bottom). For chlorophyll, the RMSe is computed for the logarithm of the concentrations, consistent with the assumption of log-normally distributed chlorophyll.*

For the RMSe of SST, the RMSe for both the analysis state and the 24-hour forecasts are shown. Overall, the assimilation of the SST leads to a strong reduction of the RMSe. On average over the full experiment period the RMSe is reduced from 0.52 °C in FREE to 0.25°C in the analysis. The 24-hour forecasts lead on average to an increase of the RMSe of 0.07°C to 0.32°C depending on days. The reduction of the RMSe relative to the free run is strongest during February and March.

Figure 4.1.2 shows the time-development of the chlorophyll and SST at the station Arkona, chosen for consistency with the 1D column experiments, for the months January to May. The figure shows the satellite observations, not in situ data. The free run shows a bloom onset from the beginning of February which declines from mid of March and appears to terminate at the end of April. The assimilation starts on February 1. Assimilating only SST observations has a negligible effect on the chlorophyll – the two curves are overlayed - consistent with the RMSe computed over the whole Baltic Sea. Constraining chlorophyll directly by assimilating chlorophyll observations reduces the concentrations from the 4th day of the assimilation process. This reduction is induced by the lower observed concentrations. However, during the second half of February and the first week of March, the modeled concentration is higher than the satellite observations. During this period the availability of satellite observations is not sufficient to fully constrain the chlorophyll. In the experiments CHL_DA and CHL+SST_DA the chlorophyll concentration declines during March consistent with the free run. However, the concentration increases again at the beginning of April. While still being lower than the concentration of the free run, the concentration from the assimilation is higher than the satellite observations. Differences between the experiments CHL_DA and CHL+SST_DA become evident from the beginning of March. Thus, the changes in the temperature field induced by the assimilation of SST observations result in a visible effect on the biogeochemistry after one month of assimilation. Over the full experiment, the root mean square error (RMSe) is reduced from 2.21 mg Chl/m^3 to 2.18 mg Chl/m^3 in SST_DA, 1.26 Chl/m^3 in CHL_DA, and 1.18 Chl/m^3 in CHL+SST_DA. Thus, the combined weakly-coupled DA of SST and chlorophyll leads to the smallest RMS error.
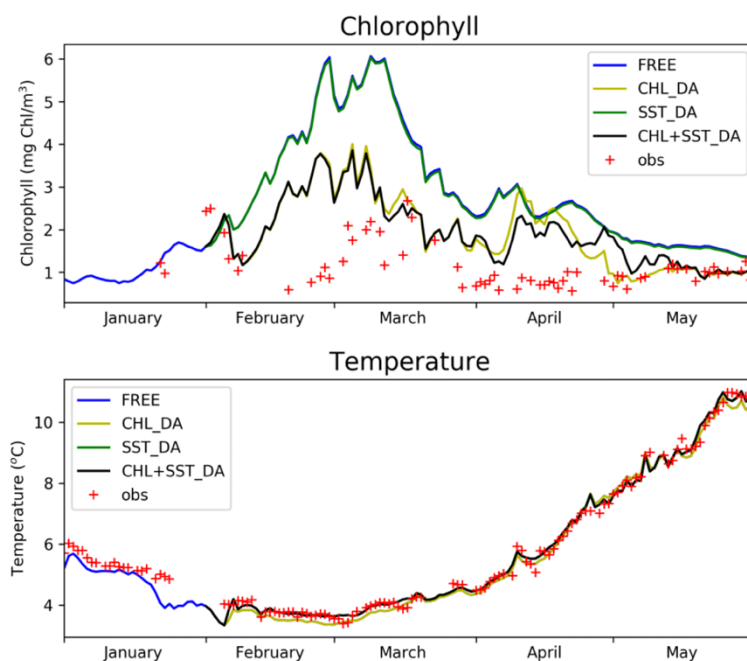

Fig. 4.1.2. *Development of the concentration of surface chlorophyll (top) and surface temperature (bottom) at the station Arkona. The lines show the different experiments: (blue) free ensemble run; (light green) assimilation of chlorophyll, (dark green) assimilation of SST; (black) combined assimilation of chlorophyll and SST. The red crosses show the satellite observations.*

The SST displayed in the lower panel of Fig. 4.1.2 shows a minimum temperature in February. After this date, the SST increases. When only chlorophyll is assimilated the SST remains unchanged as expected. Assimilating SST observations reduces the deviation between model and observations. The effect is the same in the experiments SST_DA and CHL+SST_DA. Over the full time period, the RMSe is reduced from 0.24°C in FREE to 0.18°C in SST_DA and CHL+SST_DA.

There are unfortunately no independent in situ observations of chlorophyll at the station Arkona. For this reason, we consider the alternative station Darss Sill (54.7°N, 12.7°E). The station is only about 50 km to the south-west from the station Arkona. With only 21 m depth the station Darss Sill is even shallower than the station Arkona where the depth is 45m. Figure 4.1.3 shows the concentration of surface chlorophyll (left) and surface temperature (right) at this station. The chlorophyll and temperature of the different experiments show a development over time that is very similar to that seen at the station Arkona in Fig. 4.1.2. However, in April the chlorophyll concentration is higher in the experiments CHL_DA and CHL+SST_DA compared to the free run, while it was lower at the station Arkona. The upper panels also show the values of the satellite observations. Here the time-development of the differences between the experiments and the satellite data is consistent with that discussed for the station Arkona. The lower panels of Fig. 4.1.3 show the same values for the experiments, but also in situ measurements. For the temperature, the fluctuations of the observations are higher than for the satellite data, but the values are still very close to the modeled temperatures. The in-situ measurements of chlorophyll show a larger variability than the satellite data and significantly higher concentrations in the first half of February and the first half of March. Only the free run shows comparably high concentrations, but not the same development over time as the in-situ observations. As the assimilation experiments are constrained by the lower concentrations in the satellite data, they cannot represent the peaks in the concentrations of the in-situ data.
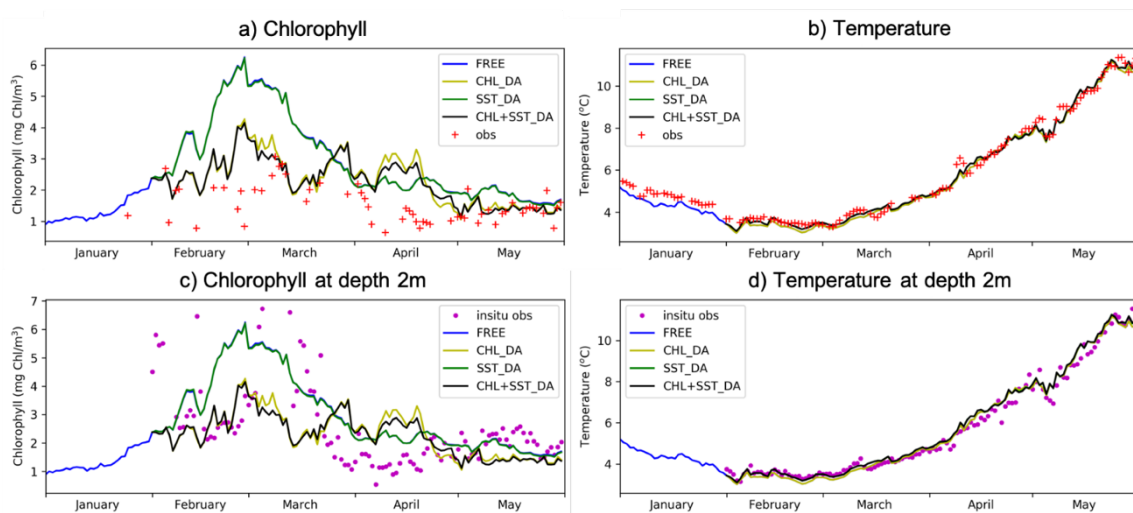

Fig. 4.1.3. *Development of the concentration of surface chlorophyll (left) and surface temperature (right) at the station Darss Sill. The line colors are analog to that of Fig. 4.1.2. The upper panels (a,b) show the values of satellite observations as red crosses. The lower panels (c,d) show the in-situ measurements at 2 meters depth as pink dots.*

Project	SEAMLESS No 101004032	**Deliverable**	D4.1
Dissemination	Public	**Type**	Report
Date	21 July 2023	**Version**	4.0

To assess the regional effects of the assimilation, Figures 4.1.4 and 4.1.5 show maps of the SST on April 1, 2015 and May 1, 2015, respectively. The assimilation leads to a better consistency between the model and the observations. The effect of the assimilation, i.e. the difference between the analysis and the forecast on this single day is small, which is the expected situation after the spin-up of the assimilation process. Panel (e) of both figures shows the difference between the free run and the 24-hour forecast from the assimilation. Here local differences up to 1.5^{o}C are visible. During March, this difference is positive almost everywhere, although lower in the location of Arkona to the South of the Baltic Sea. Thus, the effect of the assimilation is to correct a cold bias of the model. Later in the assimilation process, both positive and negative differences are visible.

The effect of the assimilation on the chlorophyll field is visible in Fig. 4.1.6, which shows the surface concentration from the four experiments and the satellite observations for May 1, 2015. As expected, the chlorophyll concentrations from the free run and the experiment SST_DA are almost identical at this time. In contrast, the assimilation of chlorophyll observations leads to significant changes. In the southern part of the Baltic Sea, the concentrations are significantly reduced compared to the free run. A reduction of the concentrations is also visible in the Bothnian Sea. In contrast, the concentrations are increased in the Gulf of Riga and the Gulf of Finland. These changes are consistent with the observations. In the Skagerrak, the observed concentrations are even lower than those in the assimilation. This difference will be corrected in the subsequent analysis step. The joint weakly coupled DA of SST and chlorophyll also leads to some visible differences from the assimilation of only Chlorophyll observations. For example, in the experiment CHL+SST_DA there are higher concentrations north of the coast of Poland and lower concentrations west of the island Gotland east of Sweden between 57°N and 58°N and south of the island Fasta Åland in the central Baltic at about 60°N.
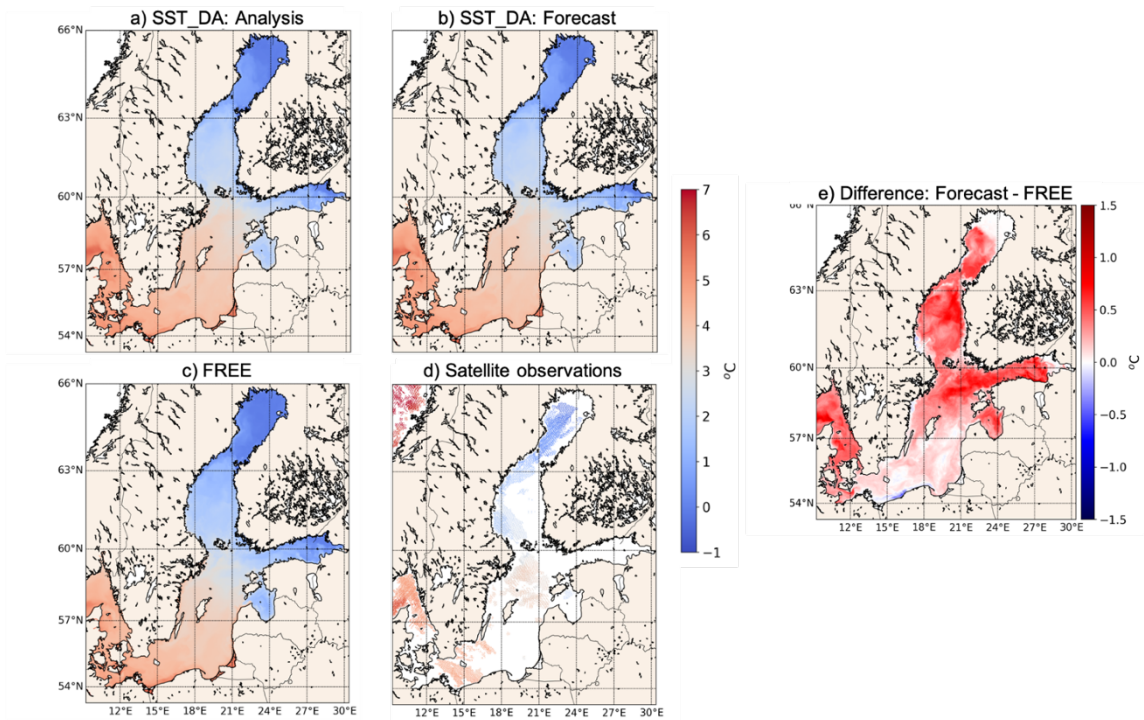
Fig. 4.1.4. *SST in the Baltic Sea on April 1, 2015 for the experiment SST_DA. Shown are the (a) 24-hour forecast, (b) analysis, (c) FREE, (d) observation, and (e) difference forecast-free.*
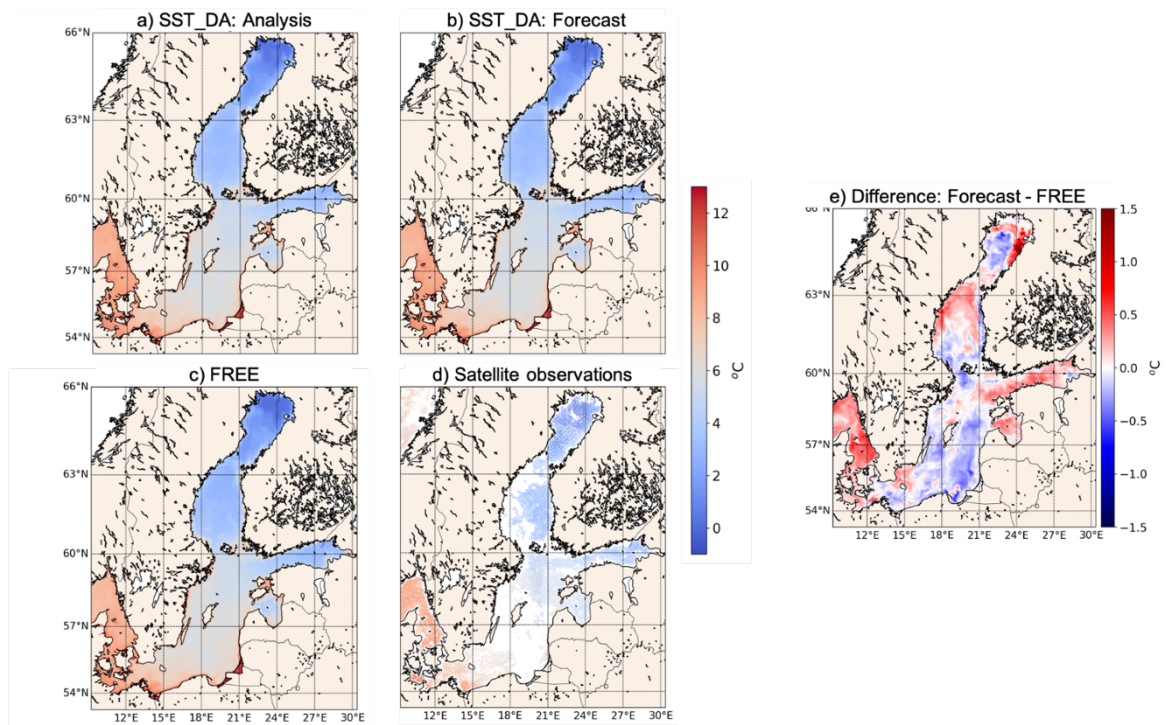

Fig 4.1.5. *SST in the Baltic Sea on May 1, 2015 for the experiment SST_DA. Shown are the (a) 24-hour forecast, (b) analysis, (c) FREE, (d) observation, and (e) difference forecast-free.*
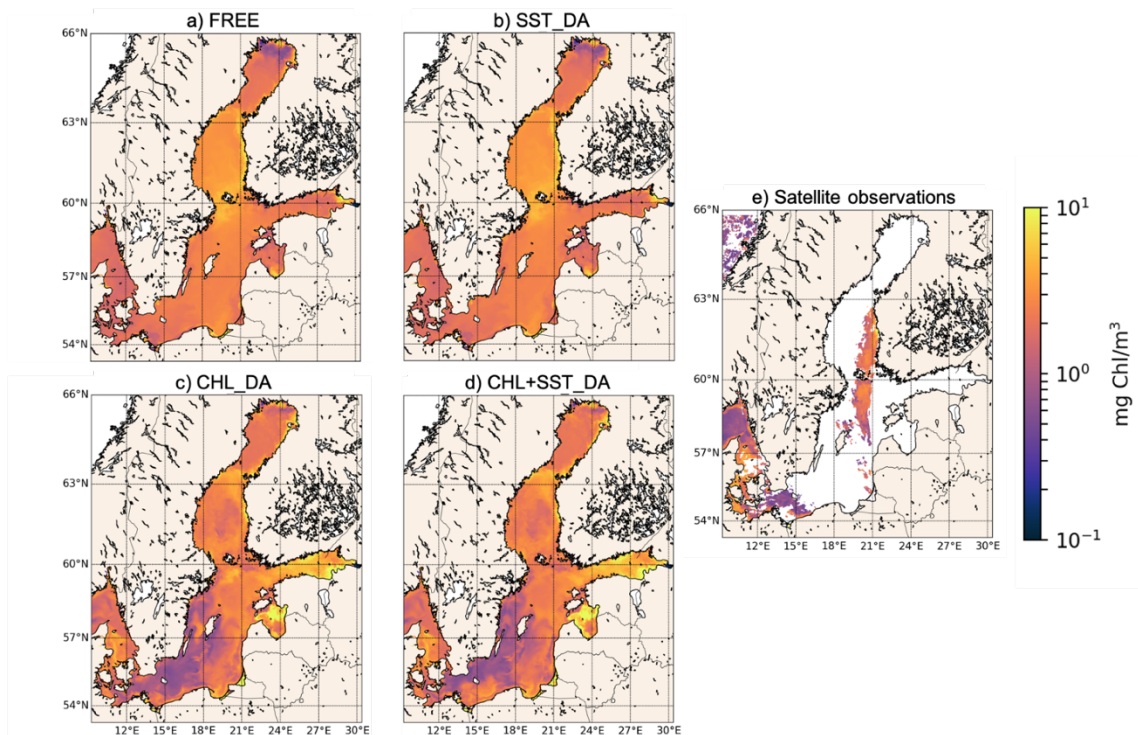
Fig. 4.1.6. *Chlorophyll in the Baltic Sea on May 1, 2015. Shown are (a) the free run and forecasts from experiments (b) SST_DA, (c) CHL_DA, (d) CHL+SST_DA, and (e) the observed chlorophyll concentration.*

Diagnostics on "non-observed" variables

With regard to non-observed variables, we first assess the effect of the data assimilation with depth. Figure 4.1.7 shows the profile of chlorophyll at the station Arkona for the free run and the 24-hour forecasts for the three assimilation experiments. Without assimilating chlorophyll observations, the differences between the experiments SST_DA and FREE are negligible. In contrast, the assimilation of surface chlorophyll leads to significant changes throughout the water column. Consistent with Fig. 4.1.2, the peak chlorophyll concentration in February and March is reduced by the assimilation. This reduction reaches down to the bottom. From end of March onwards, the concentration increases again and reaches a level comparable to the free run. In the case CHL_DA this maximum is better visible than for CHL+SST_DA. The assimilation also induces a subsurface chlorophyll maximum during May. The major differences between CHL_DA and CHL+SST_DA are visible in the upper 20m of the water column.

The changes in the chlorophyll concentration directly relate to changes in the concentrations of the three phytoplankton groups of ERGOM. These concentrations are changed in the analysis step through the ensemble-estimated cross covariances. Figure 4.1.8 shows on the left-hand side how these concentrations develop at the station Arkona over time. The concentration of diatoms, which are dominant at the beginning of March, is strongly reduced by the data assimilation. In the experiment CHL_DA the concentrations are lower than for the combined weakly coupled assimilation experiment CHL+SST_DA mainly during March.

The abundance of the cyanobacteria is negligible during the period of the experiments. The concentrations are also nearly unchanged in all assimilation experiments.
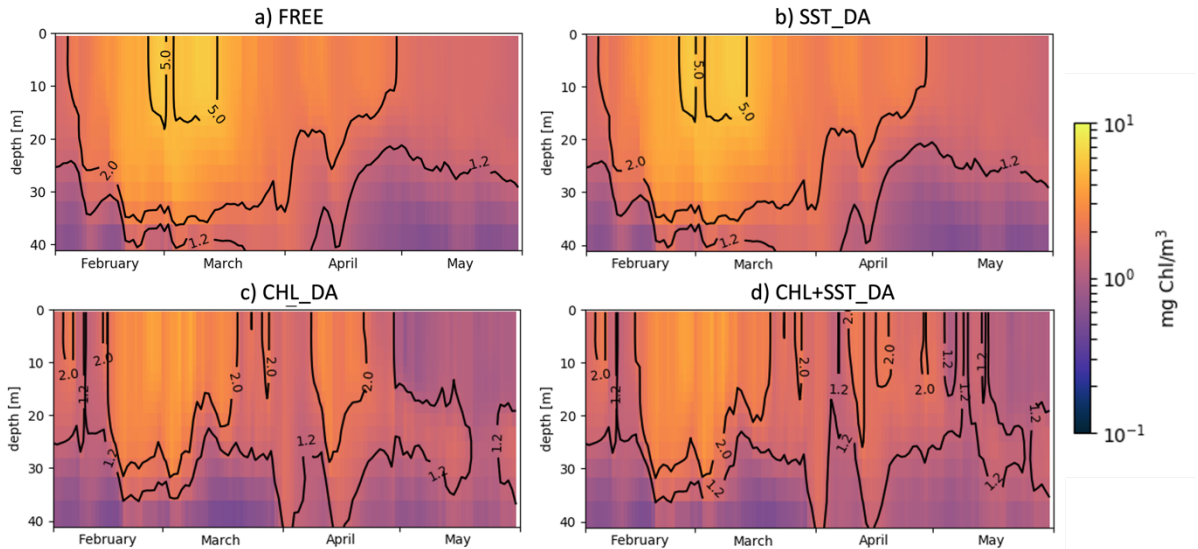

Fig. 4.1.7. *Chlorophyll concentration over depth for the period February to May 2015. Shown are the (a) free run and the 24-hour forecast for (b) SST_DA, (c) CHL_DA, (d) SST+CHL_DA.*
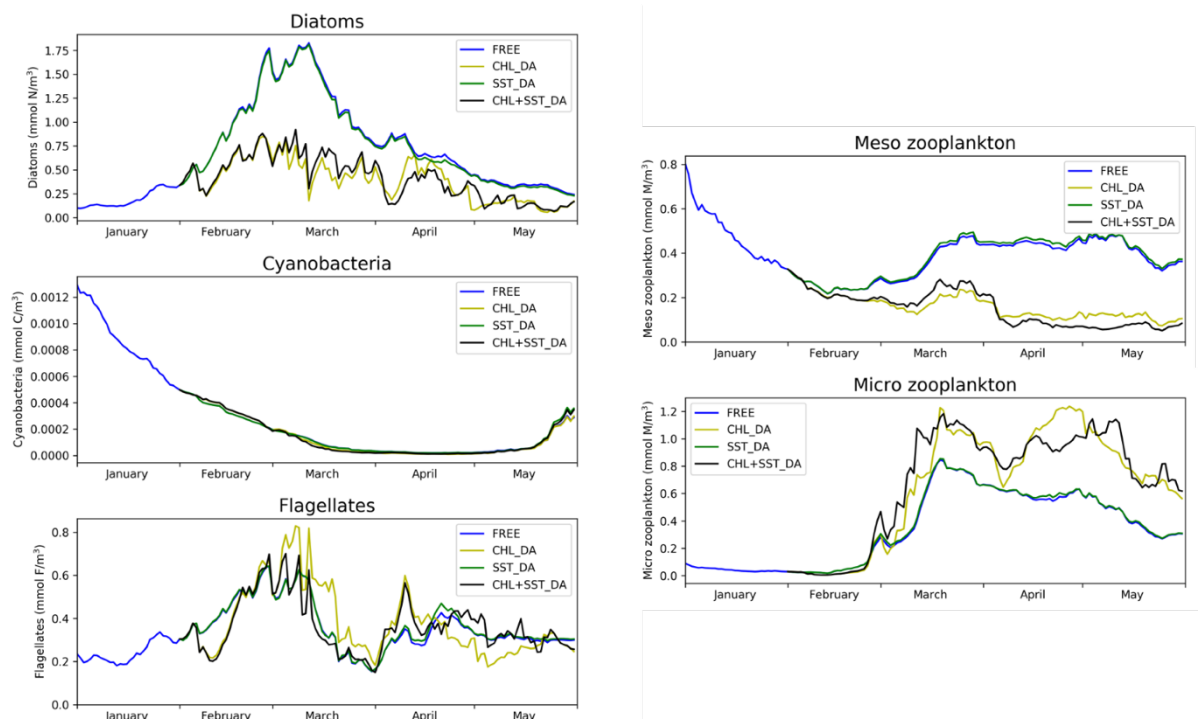

Fig. 4.1.8 *Surface concentration of the three phytoplankton groups (left) and two zooplankton groups (right) around station Arkona. The different lines show the free run (blue) and the three assimilation experiments.*

The concentration of flagellates is at a similar magnitude as that of the diatoms. However, there is no strong bloom even in the free run. When chlorophyll observations are assimilated from February 1 in the experiments CHL_DA and CHL+SST_DA the concentration is first reduced. However, the concentrations increase again from the middle of February. This might be a compensation for the strongly reduced concentrations of diatoms giving a competitive advantage to flagellates. If only chlorophyll is assimilated in the experiment CHL_DA, the concentrations of flagellates exceed the concentration obtained in the free run during March and lie below the free run from mid-April to mid-May. In the combined weakly-coupled assimilation the concentrations of flagellates remain closer to those of the free run.

The assimilation of the chlorophyll observations also changes the concentration of the two zooplankton groups both directly through the cross-covariance and through dynamic adjustments during the forecast phase. As visible on the right-hand side of Fig. 4.1.8, the concentration of the meso-zooplankton is reduced by the assimilation of chlorophyll observations, while the concentration of the micro-zooplankton is increased. Thus, the dominance of micro-zooplankton is further increased by the assimilation. When only SST observations are assimilated, the effect on the zooplankton is small, but visible, in particular for the meso-zooplankton. The combined assimilation of SST and chlorophyll in the experiment CHL+SST_DA leads to slightly different concentrations compared to the assimilation of only chlorophyll in CHL_DA. In particular, the concentration of both zooplankton groups is lower in February and March in the experiment CHL_DA compared to CHL+SST_DA, while it is larger in April and May which might be induced by the changed temperatures.

Next to the phytoplankton groups, the nutrients are directly changed by the assimilation. For the station Arkona the nutrient concentration over time is shown in Fig. 4.1.9. The assimilation of only SST has a negligible effect on all nutrients. When chlorophyll observations are assimilated, the concentrations of nitrate, phosphate and silicate are increased. The effect on silicate is particularly strong, which is likely also due to the dynamic reaction of the model on the reduced concentration of diatoms. The effect on ammonium is rather small and similar for both experiments CHL_DA and CHL+SST_DA. The joint weakly coupled assimilation of SST and chlorophyll in experiment CHL+SST_DA leads to higher concentrations of silicate from beginning of April compared to only assimilating chlorophyll. For phosphate the effect is mixed with lower concentrations for CHL+SST_DA during March and higher concentrations during April and May. A particularly large change of the concentrations is visible for the experiment CHL+SST_DA beginning of April. However, the reasons for this effect are unclear.
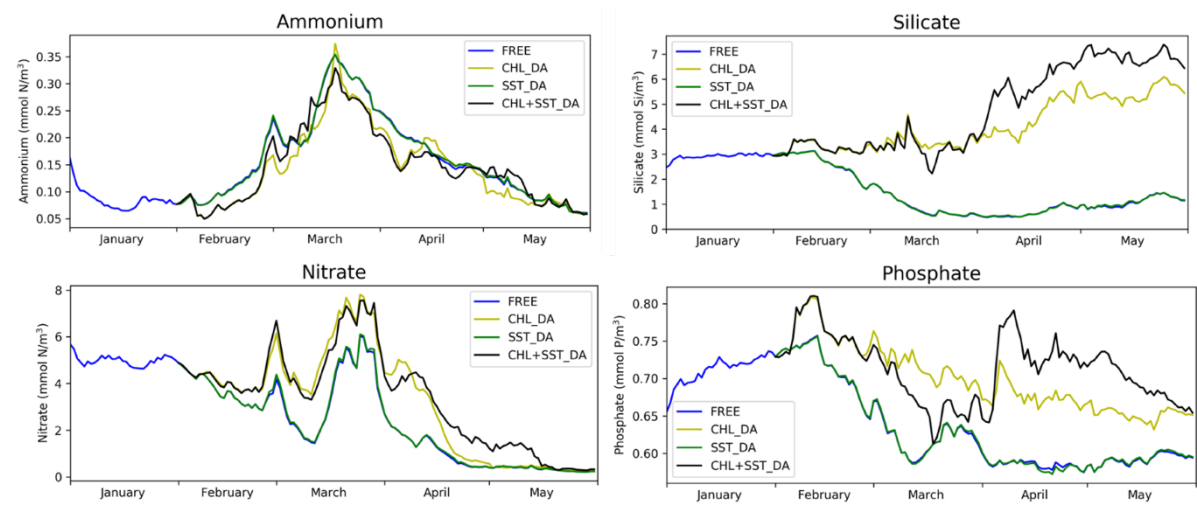
Fig. 4.1.9. *Surface concentration of ERGOM nutrients at station Arkona. Shown are (top left) ammonium, (top right) silicate, (bottom left) nitrate, and (bottom right) phosphate.*

Diagnostics on derived quantities and indicators

Here we analyze different SEAMLESS indicators: phytoplankton phenology, plankton functional types, trophic efficiency, pH, dissolved oxygen, and primary production. Due to the shallowness of the station Arkona of only 46m, we omit the POC export from the analysis.

The impact of the data assimilation on phytoplankton phenology at the station Arkona can be analyzed from Fig. 4.1.2. In particular, the data assimilation reduces the maximum amplitude of the bloom. The end of the bloom is less clear when chlorophyll observations are assimilated. While the concentrations decrease from the middle of March in the assimilation experiments analogous to the decrease in the free run, the concentrations increase again in April. Partly this development of the concentrations is also visible in the free run, but less evident due to the strong decrease in March. Nevertheless, the bloom clearly terminates end of April for all experiments. One aspect of the bloom that distinguishes the free run and experiment SST_DA from the experiments that assimilate chlorophyll is that the peak bloom duration is shortened by about 5 days with assimilation. This effect is evident from the earlier onset of the concentration decline in March. The phenology difference between the joint weakly coupled assimilation and the case CHL_DA that only assimilates chlorophyll is negligible. A possible exception is the earlier decline of the concentrations end of April in the experiment CHL_DA compared to CHL+SST_DA.

The time development of the other SEAMLESS indicators is shown in Fig. 4.1.10. The PFT ratio is generally lowered by the assimilation of chlorophyll, while the effect of only assimilating SST is negligible. The change in the PFT ratio is mainly due to the decrease of the concentration of diatoms, but also partly caused by the increase of flagellates. The trophic efficiency (TE) is increased by the assimilation of chlorophyll. Here the assimilation of only chlorophyll in CHL_DA leads to a particularly high TE in the first half of May. This appears to be mainly caused by the elevated concentration of micro-zooplankton visible in the lower right panel of Fig. 4.1.8. In the experiment CHL+SST_DA this peak is much lower and delayed by about 5 days.
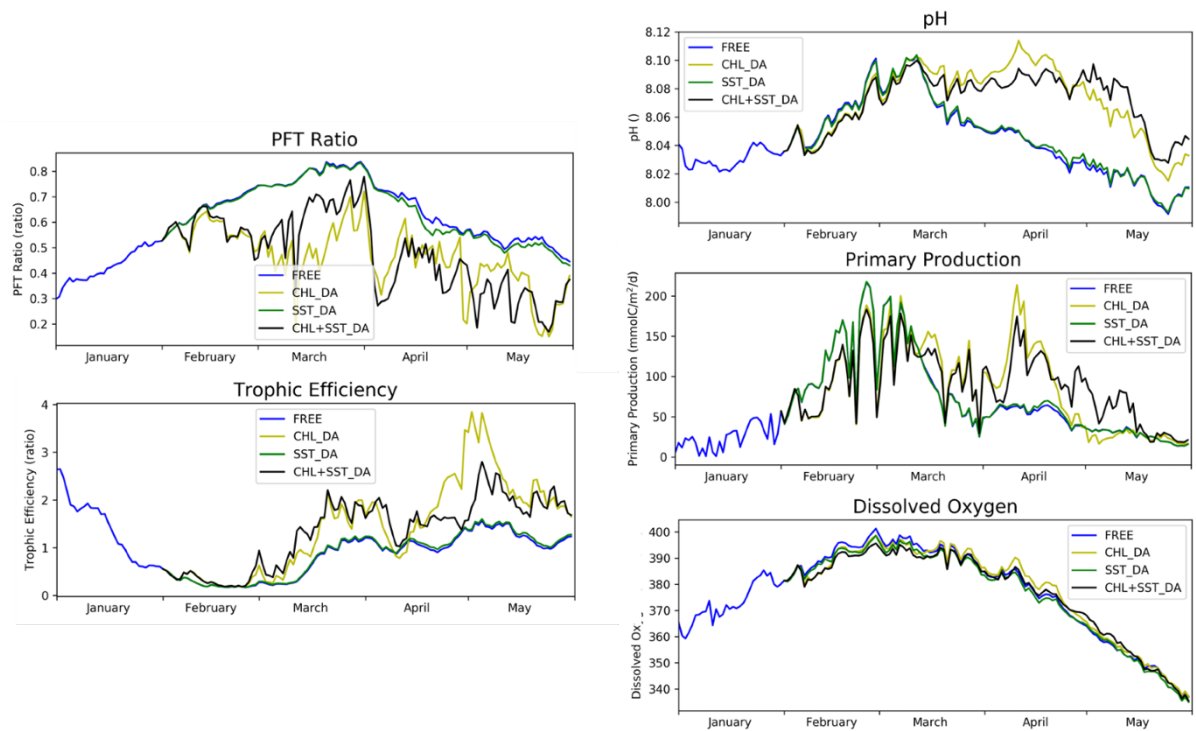
Fig. 4.1.10. *SEAMLESS indicators over time at the station Arkona.*

The assimilation leads to higher values of pH compared to the free run from the middle of March. In the free run there is a peak in pH of about 8.08 to 8.1 in the bloom in the first half of March. While the pH decreases steadily afterwards in the free run and the experiment SST_DA, the assimilation of chlorophyll observations leads to a nearly constant pH of about 8.08 until mid-May. Then the pH drops to about 8.04, which is still higher than the value of about 8.0 in the free run. This behavior is similar for the experiments CHL_DA and CHL+SST_DA, with the former showing a small peak around April 10 and a slight decline in pH afterwards.

The primary production at the station Arkona is decreased slightly in February where the initial reduction of chlorophyll, and hence the concentrations of the phytoplankton groups, reduce the primary production. However, the primary production shows a strong variability until about March 10. Afterwards, the primary production is generally increased by the assimilation of chlorophyll and shows a second peak in the middle of April. In the experiment CHL_DA, the primary production drops to the level of the free run from April 25. In contrast, the combined weakly-coupled assimilation of SST and chlorophyll leads to an increased primary production until the middle of May.

The effect on the oxygen is small for all experiments. Initially the oxygen concentration is lowered, but it is increased during April and May when chlorophyll is assimilated. Here the effect in the experiment CHL_DA is larger than in the case of the combined assimilation of SST and chlorophyll in CHL+SST_DA.

There are no observations of oxygen at the station Arkona. However, to better quantify the effect on the oxygen, Fig. 4.1.11 shows the concentration of dissolved oxygen at the station Ostergarnsholm located at 57.42°N, 18.99°E east of Gotland where in situ observations are available after February 20. The in-situ observations show a concentration between 380 and 400 mmol/m^3 for February to the

middle of May. In the second half of May, the concentration declines to about 300 mmol/m^3. The simulations generally show comparable concentrations. In April, all experiments underestimate the concentration and all fail to represent the drop in the concentration from the middle of May. The assimilation of both SST and chlorophyll has a visible effect. The combined weakly coupled assimilation shows the smallest deviation from the observations until the middle of April, when all experiments start to underestimate the dissolved oxygen concentration. The largest deviation is present in the free run. Quantitatively, the root-mean square error is reduced from 16.14 mmol/m^3 in the free run to 15.73 mmol/m^3 in SST_DA, 15.43 mmol/m^3 in CHL_DA, and 15.39 mmol/m^3 in CHL+SST_DA.
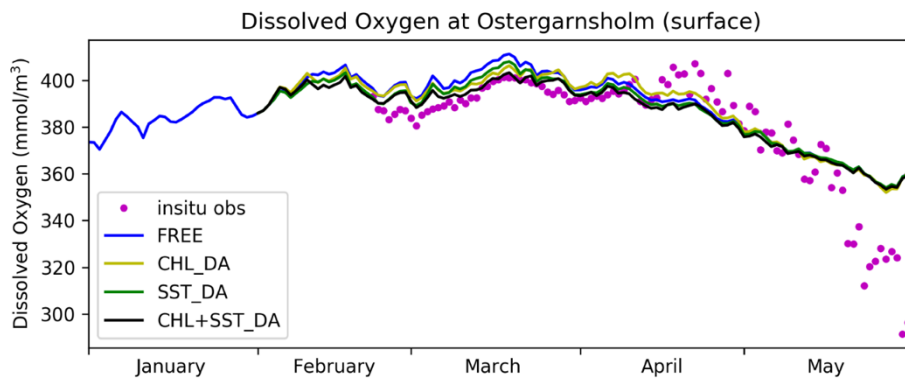
Fig. 4.1.11. *Concentration of dissolved oxygen of the surface at the station Ostergarnsholm east of Gotland.*

In order to obtain a view of the geographic distribution of the assimilation effects, Fig. 4.1.12 shows the pH over the full Baltic Sea for May 1 for the four experiments. There is a significant range of pH in the Baltic Sea with particularly high values of about 8.2 in the Gulf of Finland, and very low values of around 7.0 in the coastal area in the northern end of the Baltic Sea. In the free run, the pH in the Baltic proper is around 8.0. The assimilation of only SST leads only to minor changes. When only chlorophyll observations are assimilated, the pH is increased to about 8.2 in the northern part of the Baltic proper and along the southern coast of the Baltic. This effect is also present, but lower and more constrained to the Gulf of Finland and the southern coastal region of the Baltic, when both SST and chlorophyll are assimilated.
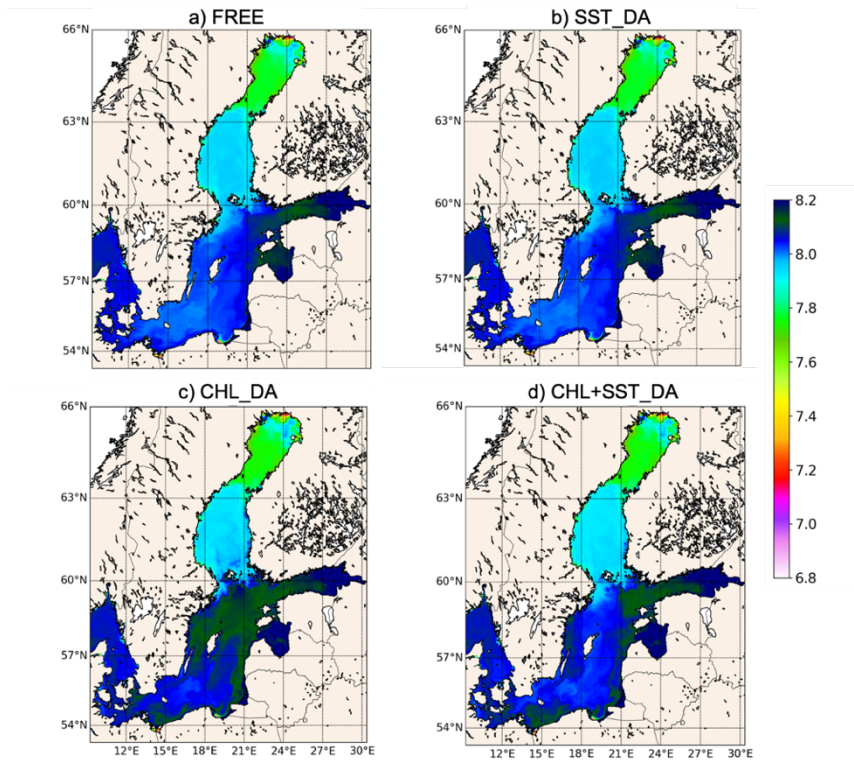
Fig. 4.1.12. *pH at the ocean surface on May 1, 2015. Shown are the free run (top left), SST_DA (top right), CHL_DA (bottom left) and CHL+SST_DA (bottom right).*
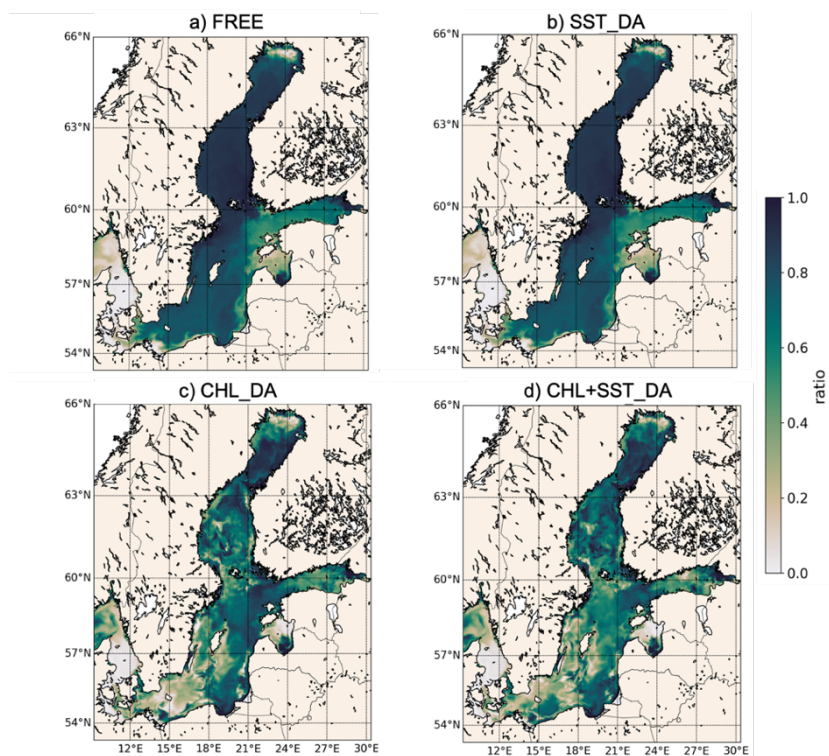

Fig. 4.1.13. *PFT ratio at the ocean surface on May 1, 2015. Shown are the free run (top left), SST_DA (top right), CHL_DA (bottom left) and CHL+SST_DA (bottom right).*

The effect of the assimilation on the PFT ratio is shown in Fig. 4.1.13. Consistent with the previous analysis, the effect of assimilating only SST observations is negligible for the PFT ratio. The assimilation of chlorophyll observations reduces the PFT ratio in most regions. Here the reduction is stronger in the Baltic Proper in case of the combined weakly coupled assimilation of SST and chlorophyll in experiment CHL+SST_DA. In the southern part of the Baltic between Poland and Sweden, the reduction is stronger when only chlorophyll is assimilated. At the western end of the Gulf of Finland the PFT ratio is increased by the chlorophyll assimilation.

Finally, we assess the trophic efficiency (TE) in the Baltic Sea. Figure 4.1.14 shows that on May 1, the TE is generally below 0.5 in most of the Baltic Sea when no observations are assimilated. Larger TE is only visible in the Gulf of Finland and in particular in the Skagerrak and Kattegat. The effect of assimilating SST is negligible while the assimilation of chlorophyll observations increases the TE in the southern half of the Baltic Sea. Here, the effect is larger when only chlorophyll is assimilated compared to the combined weakly coupled assimilation of SST and chlorophyll.

Overall, the analysis shows significant differences between the assimilation of only chlorophyll observations and the joint weakly coupled assimilation of both SST and chlorophyll. The experiments show that the assimilation of chlorophyll is essential to constrain the ecosystem variables of ERGOM, since the effects of assimilating SST observations alone are negligible for the ecosystem variables and indicators. However, in combination the effects of SST and chlorophyll observations are larger. Overall, the combined assimilation leads to the best representation of the ecosystem variables as well as the temperature field.
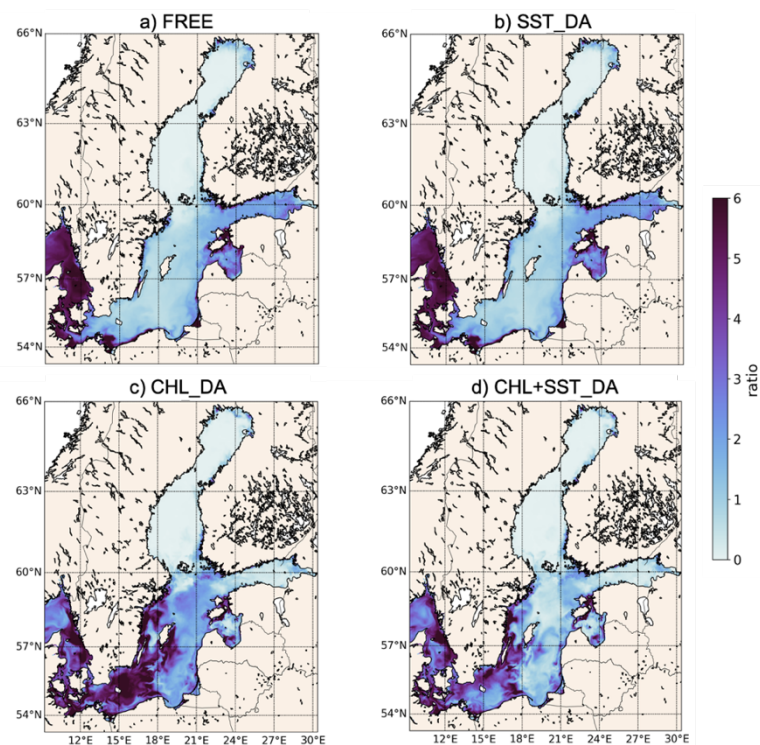

Fig. 4.1.14. *TE at the ocean surface on May 1, 2015. Shown are the free run (top left), SST_DA (top right), CHL_DA (bottom left) and CHL+SST_DA (bottom right).*

4.2 Assimilation results in the GLO/IBI MFC domain

In this section we present the results obtained by **IGE/UGA** as part of Task 4.1a using the assimilation method described in Deliverable 3.4 and the weakly coupled experimental design described in Section 3.2.

Diagnostics on observed variables

The prior distribution is first conditioned by along-track altimeter data, resulting in the reduction of RMS statistics as illustrated by Figure 4.2.1. The posterior statistics (after the first update) are consistent with an expected error of ~ 3cm in average (ensemble mean RMS error < 5 cm). The RMS difference with independent AltiKA measurements demonstrate an effective error reduction during the hindcast period, which disappears after a few days of statistical forecasting. The corresponding ensemble mean of the reconstructed SSH is illustrated by Figure 4.2.2 for the situation of May 1st, showing a well-marked cyclonic eddy in the north-western corner of the domain. The ensemble mean SSH pattern is corroborated by the more smoothed L4 SSH CMEMS product, based on objective analysis of the same altimeter tracks. Hence, this first inversion allows us to improve the localization and strength of mesoscale structures.

The histograms shown in Figure 4.2.3 suggest that: (i) in terms of SSH, the prior ensemble distributions during the hindcast and forecast periods are overall consistent with independent (non-assimilated) altimeter data, except for a few extreme outliers, (ii) the posterior SSH ensemble distribution during the hindcast period (centred on April 20th) has essentially removed the outliers in the highest rank, and (iii) the posterior SSH ensemble distribution during the forecast period (centred on May 30th) is showing an increased over-dispersive (underconfident) tendency of the ensemble.
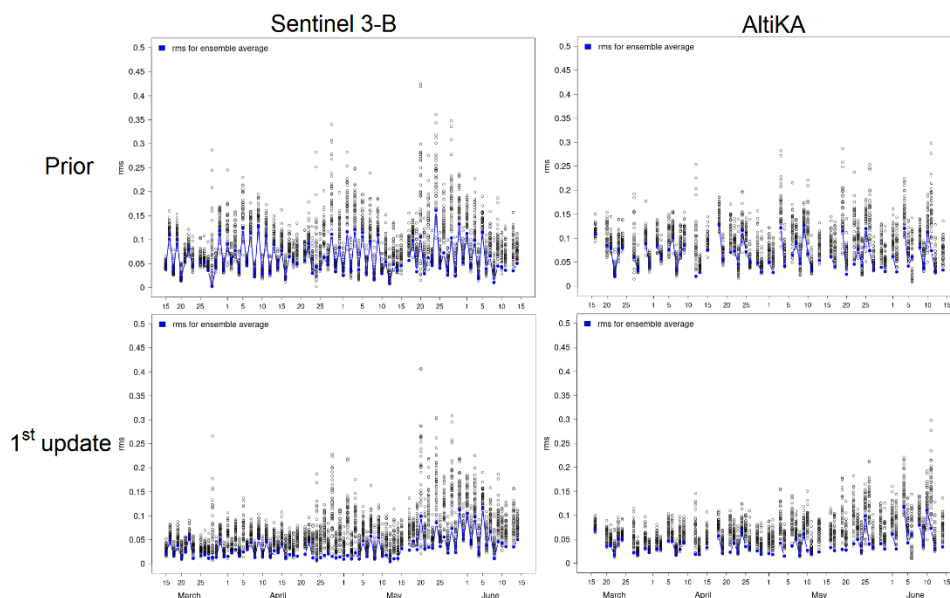

Figure 4.2.1: *RMS error statistics on SSH (in meter) computed daily during the 3-month experiment between ensemble members, ensemble mean (in blue) and assimilated Sentinel-3B (left) and non-assimilated AltiKA (right) altimeter data for the prior and first updated distribution.*
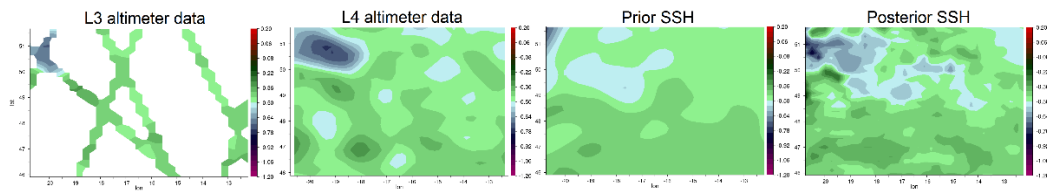
Figure 4.2.2: *SSH (in meter) in the PAP region for May 1st. From left to right: assimilated along-track CMEMS L3 SSH data; non-assimilated CMEMS L4 SSH data; ensemble mean of the prior distribution; ensemble mean of the posterior distribution.*
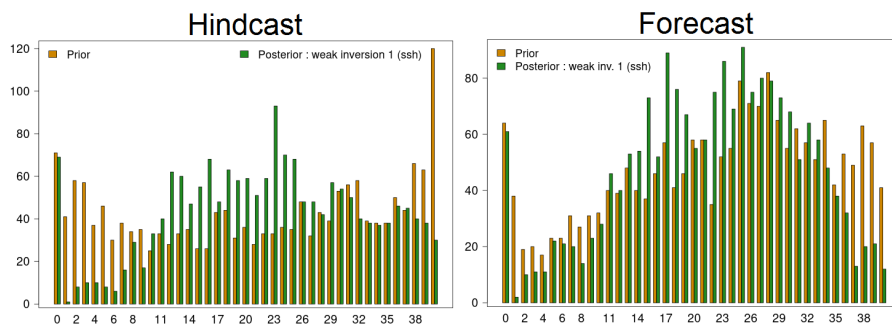

Figure 4.2.3: *Rank histograms for the PAP region calculated with the 2 non-assimilated satellite data sets (AltiKA, Cryosat-2) for 11-days periods in the hindcast (left) and forecast (right) periods. The brown bars represent the prior ensemble, the green bars represent the posterior ensemble after first observational update by altimetric data.*

The impact of weakly coupled assimilation on surface chlorophyll after the first update (i.e. using SSH data only) is slightly positive during the very early stage of the spring bloom, bringing all members closer to L4 OC observations and removing several outliers of the distribution (Figure 4.2.4). However, the impact quickly becomes negligible when the bloom intensifies after mid-April. This result is plausible given the weak co-variability between the SSH and surface chlorophyll patterns observed in the data set for the different dates.

Further, Figure 4.2.4 shows that the second update of the distribution by OC data is necessary to significantly reduce the spread of ensemble members during the hindcast period. RMS statistics confirm the smaller misfit between ensemble members and L4 OC data during the spring bloom hindcast. These findings for the region around PAP suggest that the posterior ensemble contains more faithful information about indicators such as phenology. Indicatively, the ratio of the posterior/prior ensemble variance used to quantify the reduction of uncertainty (see D3.4) is 0.321 at PAP station, i.e., a reduction of 43.3% of the ensemble standard deviation in the anamorphic space assuming 30% observation error variance. At local scale, some positive effects of the conditioning by OC data are detectable during the first 5-10 days of the forecast period, though probably not very significant.

Figure 4.2.5 illustrates the reconstruction of surface chlorophyll patterns during the hindcast period. It can be observed that (i) the range of chlorophyll values in the posterior distribution agrees with L3 or L4 products over the domain (this was not the case for the prior distribution), and (ii) the consistency between observed and reconstructed spatial structures in cloud-free regions seems to be

improved. During the forecast period (see Figure 4.2.6), the reconstruction suggests some limited skill in the south-east corner of the domain with a few days of lead time, while some unrealistic chlorophyll spots develop along the northern boundary.
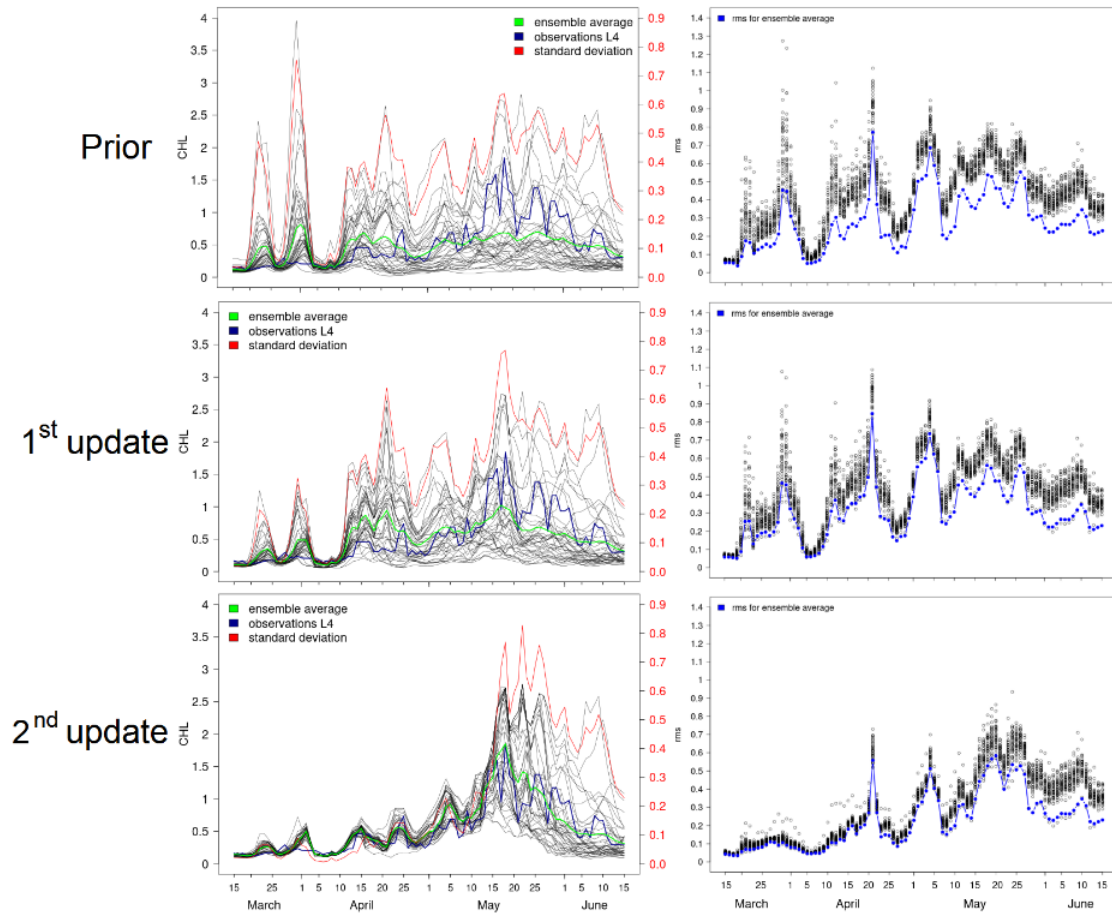

Figure 4.2.4: *Time series of the surface chlorophyll concentration (in mg/m3) at 16°30' W, 48°50'N (PAP station) for the prior (upper left), first (central left) and second posterior (lower left) ensembles. The black curves show the 40-member ensemble; the green curve is the ensemble mean; the blue curve is the L4 CMEMS OC product collocated at PAP; the red curve is the standard deviation. On the right column are shown the RMS between L4 CMEMS OC product, the ensemble members and the ensemble mean of surface chlorophyll concentration (in mg/m3) over the analysed region around PAP.*
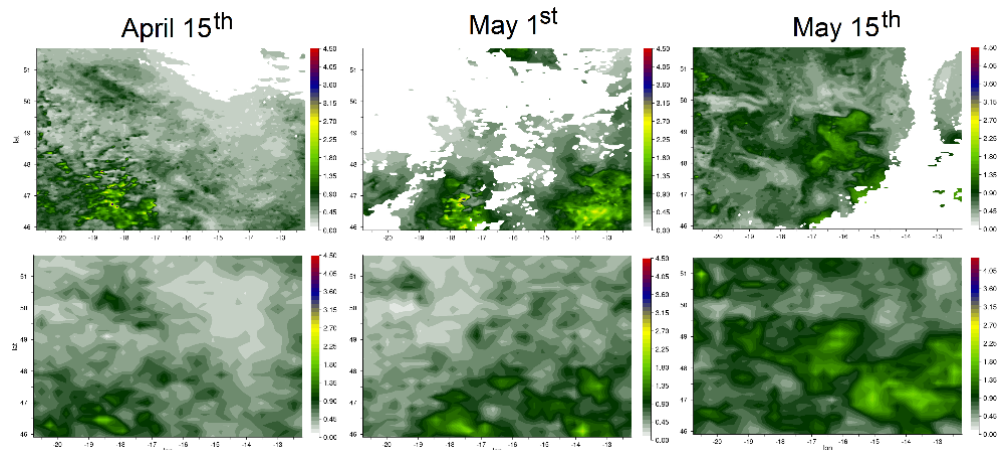
Figure 4.2.5: *Surface maps of chlorophyll concentration (in mg/m3) in the PAP station area (1100 km x 720 km centred on 16°30' W, 48°50'N) during the hindcast period (from April 15th to May 15th): assimilated CMEMS L3 product at 4km resolution (impacted by clouds) (upper row); posterior ensemble mean (lower row).*
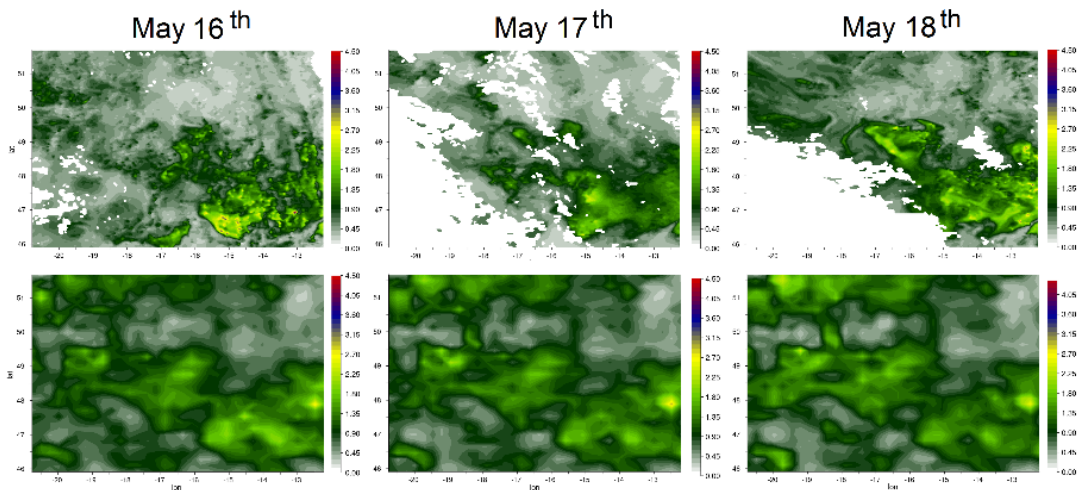

Figure 4.2.6: *Surface maps of chlorophyll concentration (in mg/m3) in the PAP station area (1100 km x 720 km centred on 16°30' W, 48°50'N) during the first 3 days of the forecast period: non-assimilated CMEMS L3 product at 4km resolution (upper row); posterior ensemble mean (lower row).*

In the PAP region, when the simulated sources of uncertainty are limited to horizontal grid location, sub-grid scale effects and 10 uncertain PISCES BGC parameters, we conclude that the impact of OC data strongly dominates the effect of SSH data assimilation. The benefits of the two successive updates (as described in the corresponding algorithm, see section 3) based on satellite altimetry and ocean colour data are cumulative, with no degradation due to the assimilation of SSH data as is often reported with current operational systems. This already represents a promising step forward, and justifies the implementation of the 4D method in other regions where the co-variability between SSH and OC is stronger.

Diagnostics on "non-observed" variables

Since only surface data are assimilated in these experiments, it is interesting to diagnose how the surface information allows to constrain unobserved tracers such as nutrients and chlorophyll in the sub-surface euphotic zone. This is illustrated by Figures 4.2.7 and 4.2.8 for 3 dates, 5 days apart. The ensemble vertical profiles show a well-developed phytoplankton bloom that coincides with depleted NO3 in the upper 40 meters. In the hindcast period (May 10th), the assimilation reduces the spread of chlorophyll profiles by a factor of 3. The signature of a weak DCM around 25 meters is slightly enhanced but the depth of the productive layer is unchanged. The spread of the nutrient profiles is reduced less (~ factor 2) and the ensemble mean is nearly unchanged. After a 5-days forecast (May 20th), the assimilation impact is overall small: the posterior ensemble spread is slightly larger than the prior, the weak DCM has disappeared from all members, and the mean chlorophyll concentration is increased. In the same time, the mean NO3 value in the mixed layer is reduced. The impact at the end of the hindcast period (May 15th, with only past data being assimilated) is intermediate in terms of spread but the mean chlorophyll concentration is more than doubled. Nutrients are nearly unaffected.
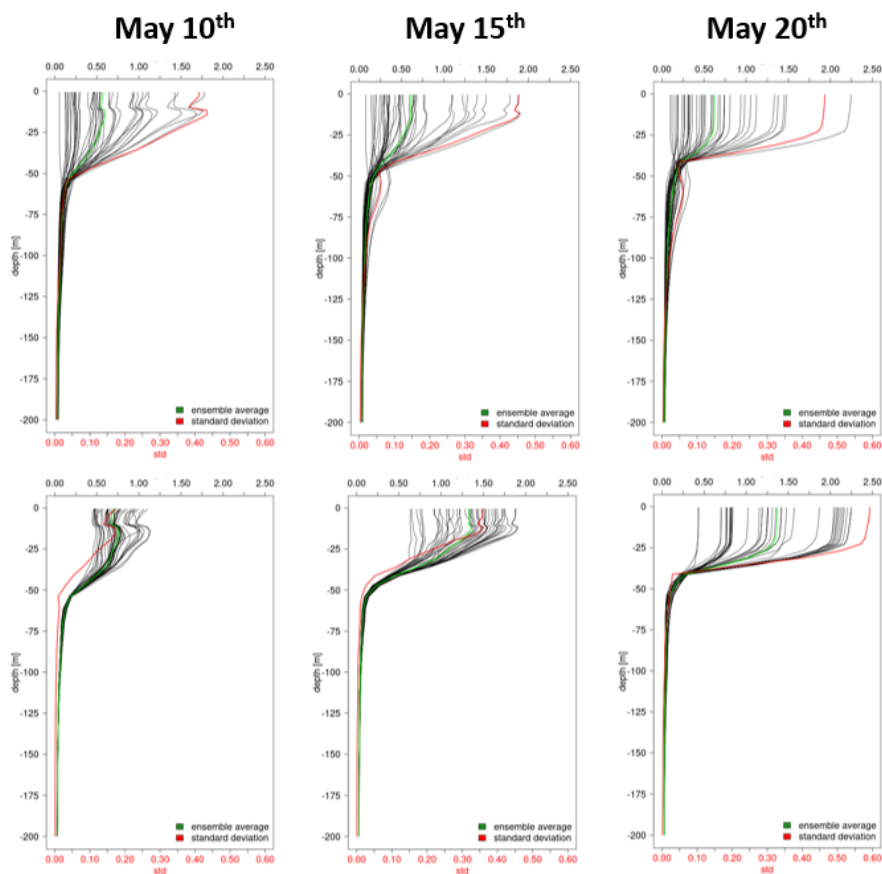

Fig. 4.2.7. *Prior (upper row) and posterior (lower row) distributions of vertical chlorophyll profiles at 16°30'W, 48°50'N (PAP station) for May 10th, 15th and 20th. The black curves are the vertical profiles of the 40 ensemble members; the green curves are the ensemble mean; the red curves are the ensemble standard deviation.*

These results are difficult to interpret mechanistically, but they suggest that the OC information is propagated to several BGC variables according to the ensemble statistics, modifying the stocks in the euphotic zone without changing significantly the shape of their vertical structure. Further, it can be noted that the prior assimilation of physical data does not seem to introduce obvious inconsistencies in the BGC variables associated to, e.g., spurious vertical mixing.
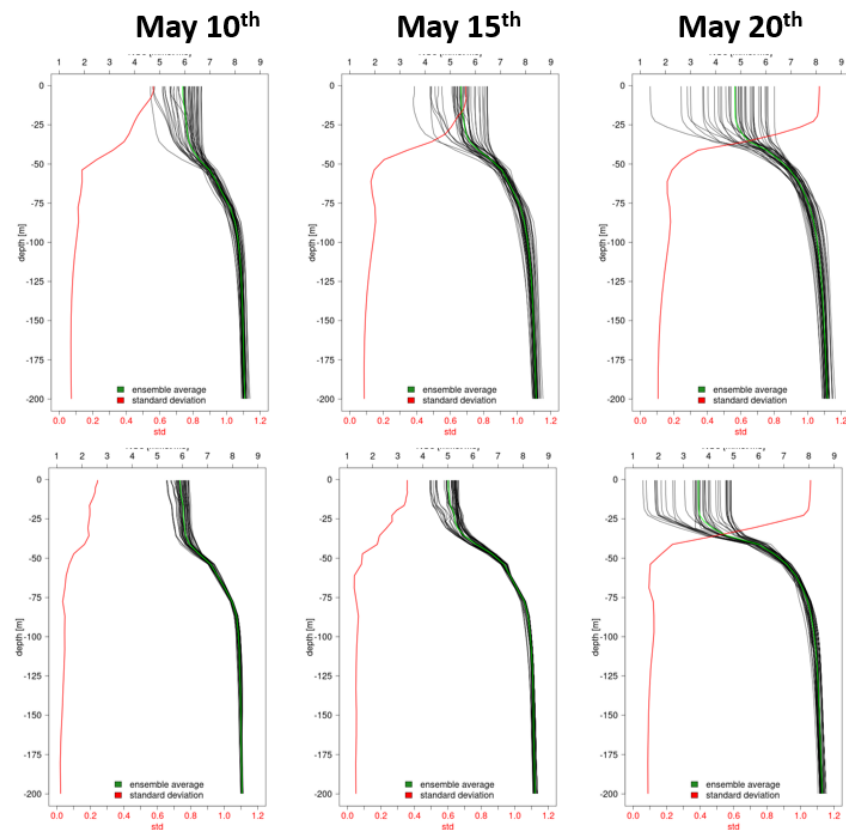

Fig. 4.2.8. *Prior (upper row) and posterior (lower row) distributions of vertical NO3 profiles at 16°30'W, 48°50'N (PAP station) for May 10th, 15th and 20th. The black curves are the vertical profiles of the 40 ensemble members; the green curves are the ensemble mean; the red curves are the ensemble standard deviation.*

Diagnostics on derived quantities and indicators

The 3-month weakly coupled assimilation experiment is finally assessed in terms of impact on SEALMESS indicators related to phytoplankton dynamics: downward flux of particulate organic carbon (POC) at 100 meters, Trophic Efficiency in the upper 200 meters and vertically integrated Primary Production.

The statistics shown in Fig. 4.2.9 for the PAP station confirm that, during the spring period, the biogeochemical processes at depth are significantly influenced by the plankton dynamics in the upper layer when constrained by assimilated surface data. The variance reduction is significant for the 3 indicators throughout the hindcast period and becomes negligible after a few days of forecasting. The

ratio between posterior and prior ensemble variance for POC (0.361) on May 15th is similar to the corresponding value obtained for Surface Chlorophyll (0.321), while the ratio for Trophic Efficiency and Primary Production is smaller.

The diagnostics on observed variables as previously discussed suggest that this is mainly the result of assimilated ocean colour data, while altimetry has a very weak impact on the posterior distributions. The similarities between the temporal evolution of the 3 indicators obtained with "uncoupled" assimilation during the hindcast period (see D3.4) and the weakly coupled assimilation estimates shown in Figure 4.2.9 confirm this assessment.
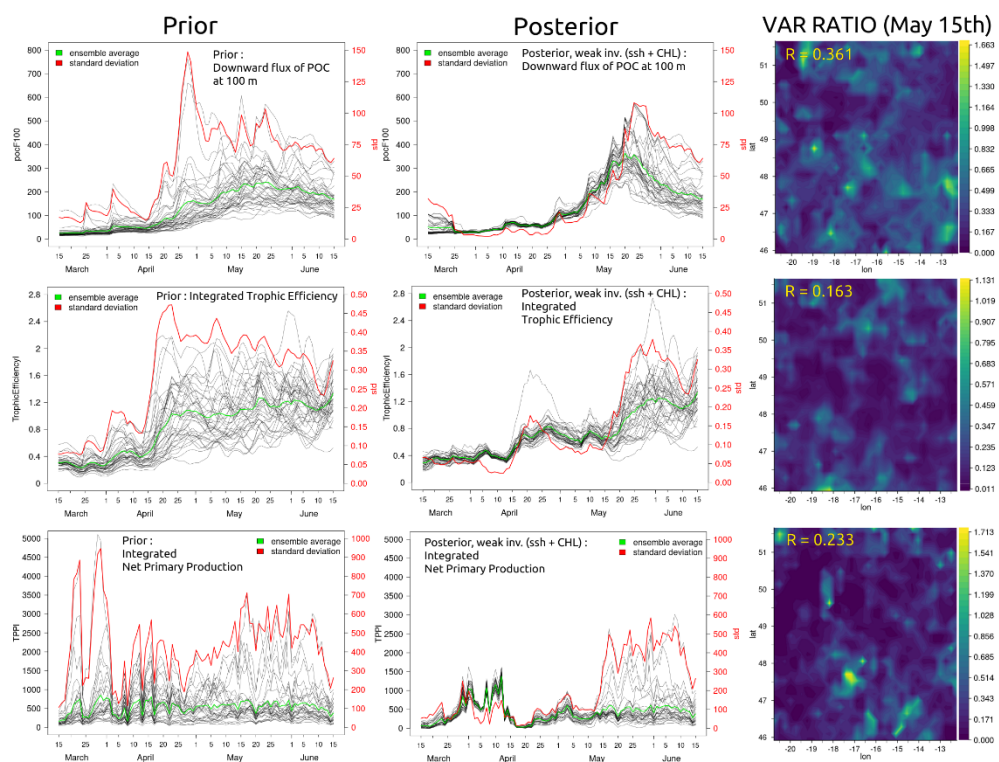

Fig. 4.2.9. *Time series of (i) (upper row) downward flux of the particulate organic carbon at 100-meter depth (in mg.C/m2/day); (ii) (middle row) Trophic Efficiency (ratio of vertically integrated values of total zooplankton and phytoplankton biomass between 0- and 200- meter depth) and (iii) (lower row) vertically integrated total Primary production (in mg.C/m2/day) at 16°30' W, 48°50'N (PAP station), for the prior (left panel) and posterior (central panel) ensembles of weakly coupled assimilation experiments. The black curves show the 40-member ensemble; the green curve is the ensemble mean; the red curve is the standard deviation. Right panel: ratio between posterior and prior ensemble variance in the region around PAP on May 15th (R is the average ratio over the area).*

As for the uncoupled assimilation experiments reported in D3.4, it should be recalled that the interpretations and statistics obtained on the derived quantities are based on quite specific assumptions about the sources of uncertainty and the way they are accounted for in the NEMO/PISCES stochastic model. These could only be confirmed with verification data which, however, are not available for the considered SEAMLESS indicators. The conclusions that can be drawn about the benefit of weakly coupled assimilation when compared to OC-only assimilation therefore remain

highly speculative. The comparison between weakly and strongly coupled assimilation experiment will be further developed in D4.2.

4.3 Assimilation results in the NWS MFC domain

Diagnostics on observed variables

As part of the WP3 we have demonstrated that for the assimilation of satellite ocean-colour (OC) chlorophyll, the hybrid ensemble-3DVAR system from SEAMLESS improves simulated chlorophyll relative to the existing 3DVAR operational system. However, including also the weakly coupled assimilation of physical data has a major impact on the simulated chlorophyll even when we simultaneously constrain chlorophyll through the assimilation of satellite OC data. This is very different from the 3DVAR system where such impact has been demonstrated to be negligible. The overall chlorophyll is substantially larger when physical data are assimilated into the model (Fig. 4.3.1), however the impact of physical DA is constrained dominantly to the sub-surface chlorophyll.
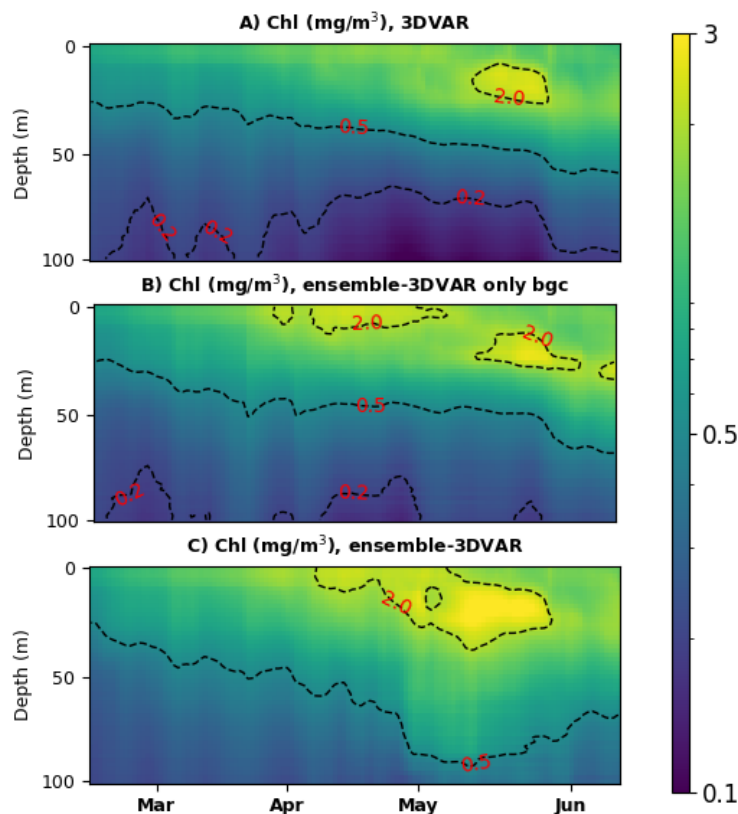

Figure 4.3.1: *Hovmoller plot showing simulated chlorophyll horizontally averaged across the NWE Shelf. The top panel shows the 3DVAR operational set-up, the middle panel the hybrid system assimilating only OC chlorophyll and the bottom panel the weakly coupled physical-OC chlorophyll DA run using the hybrid system. (The Figure was shown as Fig. 4.3.4 in Deliverable 3.4.)*

To understand the different impact of physical DA on biogeochemistry, we investigated the differences between the 3DVar and ensemble-3DVar produced physics analyses, looking both at the physical variables (temperature, salinity, velocity components), as well as temperature innovations

and increments. In the physical component of the coupled model the temperature shown in Fig. 4.3.2 displays almost no difference between the 3DVAR and the new hybrid ensemble-3DVAR reanalyses. Similarly, looking at the size of temperature DA increments, which are expected to be the original driver behind the mixing changes, they appeared to be larger for hybrid DA than 3DVAR only near the surface, but are very similar in >30m depth. Furthermore, the vertical speed of the sub-surface currents appeared to be only slightly larger in 3DVAR than in the hybrid DA run, but not dramatically different either.
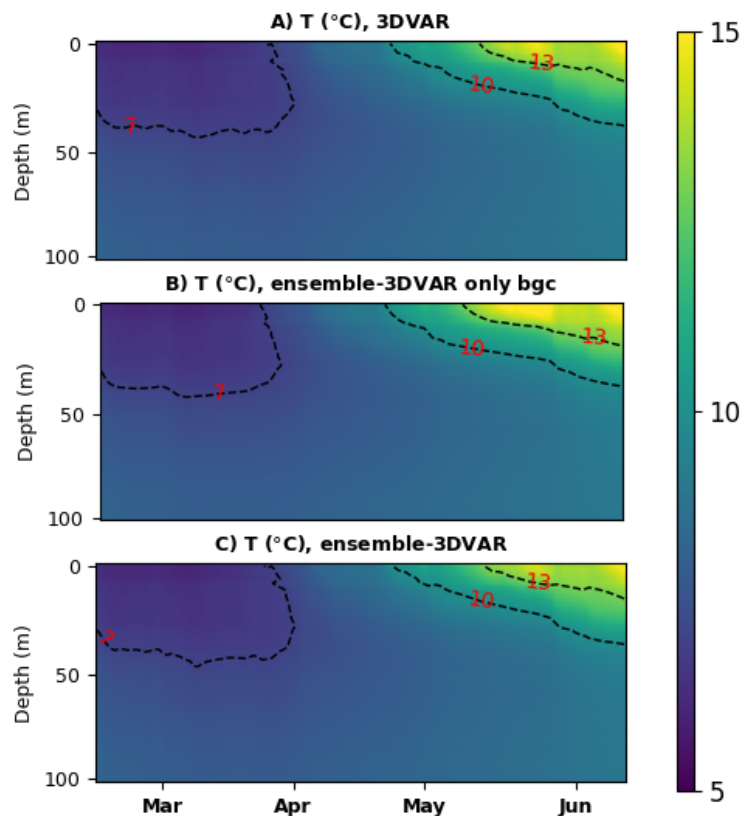

Figure 4.3.2: *Similar Hovmoller plots as in Fig.4.3.1, but for temperature instead of chlorophyll.*

The validation using glider data from the field campaign of the NERC AlterEco project in the North Sea showed that the weakly coupled run mostly degrades the simulated chlorophyll with respect to both the hybrid run assimilating only OC chlorophyll and the weakly coupled 3DVAR system (Fig. 4.3.5 from Deliverable 3.4). The comparison is always done with the ensemble mean, but there are no major differences between the ensemble mean and median, suggesting that the posterior PDF is not significantly skewed. It needs to be said that the there is only very limited amount of validation data, with different types of data (glider, L4, NSBC) yielding qualitatively different results. Our concluding remarks will be based on the glider data which seemed the most robust and appropriate, but they are still very limited spatio-temporally.

We suggest the following explanation of the chlorophyll differences between the weakly coupled 3DVar and ensemble-3DVar simulation: the physical DA seems to moderately degrade simulated

chlorophyll also in the 3DVar case. This is shown by the Fig. 10:A (including the same glider data) of the recent study by Skakala et al. (2022). However, in case of including into the 3DVar system also OC chlorophyll assimilation, the overestimates of the background variances by the climatologies supplied to the 3DVar system, cause the chlorophyll from the reanalyses converge to the assimilated observations (this has been discussed in various studies, e.g. Skakala et al, 2020, 2021, 2022). This happens irrespectively of physical DA and effectively ``overwrites'' the (mostly negative) impact of the assimilated physics on chlorophyll (again see Fig. 10:A of Skakala et al, 2022). However, ensemble-3DVar chlorophyll assimilation constrains the simulated chlorophyll less tightly than the 3DVar system (Fig. 4.3.1 of Deliverable 3.4), due to the improved flow-dependent estimates of the background covariances. This appears to have mostly beneficial impact on chlorophyll (e.g. Fig. 4.3.5 of Deliverable 3.4). However, in the situation when also physics is assimilated into the model the weaker impact of the chlorophyll assimilation in the ensemble-3DVar system turns out to be unable to fully compensate for the (negative) impact of the physical DA on chlorophyll. The issue is quite fundamental and can be improved in one of three ways: 1) through improving the interplay between physics and biogeochemistry in the model, 2) through improving the realism of physics DA, or 3) through the strongly coupled DA system.
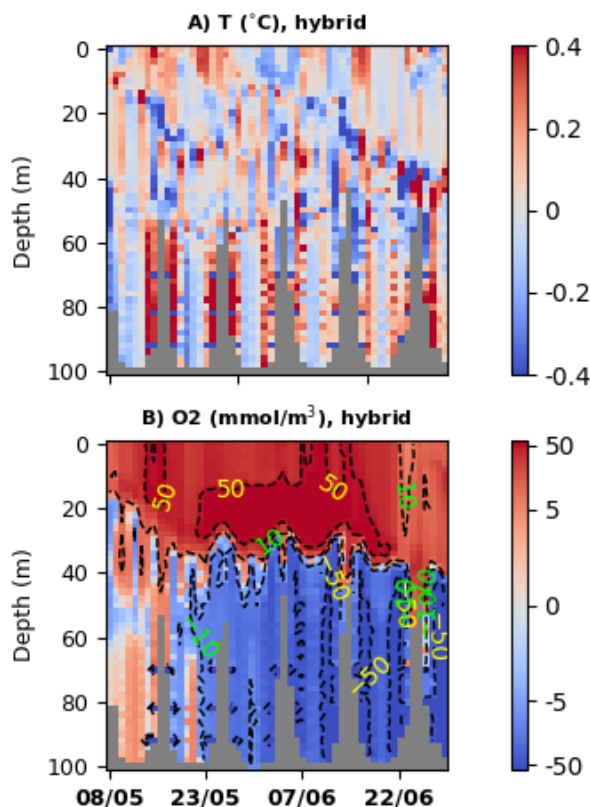

Figure 4.3.3: *Hovmoller plots comparing the weakly coupled run using the hybrid system with the AlterEco glider (reanalysis minus glider) for temperature (upper panel) and oxygen (bottom panel). A figure showing chlorophyll comparison was published in Deliverable 3.4.*

As for other variables than chlorophyll, Figure 4.3.3, upper panel, shows the validation of temperature using the data from the same glider mission. Unfortunately, the 3DVAR simulation, used here typically as a reference, assimilated also the glider data for temperature and chlorophyll from May-June period of the AlterEco mission (otherwise it was a precise analogue of the hybrid run). The glider data were spatially very limited, so for shelf-wide comparisons they have negligible impact, but the skill of the reference 3DVAR run cannot be sensibly compared to the hybrid run when the same glider data are used for model validation.

Diagnostics on non-observed variables

The only non-observed variable for which we had reasonable validation data was oxygen. The results are shown in Fig. 4.3.3, bottom panel. These oxygen reanalysis-observation match-ups are comparable with a 3DVAR reanalysis assimilating OC satellite chlorophyll and slightly better than the model free run (see Fig. 11 of Skakala et al. (2021) for comparison). They are however slightly worse than for the ensemble-3DVar run assimilating only OC chlorophyll (Fig. 4.3.7 of Deliverable 3.4), which can be explained by the relative degradation of chlorophyll (and therefore phytoplankton biomass/primary production) in the weakly coupled run.

Diagnostics on derived quantities and indicators

As far as the SEAMLESS indicators are concerned, we have found that under the weakly coupled DA of physical data and total chlorophyll we can ``observe'' phytoplankton phenology, oxygen, net primary production, POC and trophic efficiency, while it has more moderate impact on phytoplankton community structure, pH and bottom oxygen (see Fig. 4.3.4).

Fig. 4.3.4 demonstrates that the weakly coupled ensemble-3DVAR substantially reduces the intense phytoplankton bloom in the ERSEM free run, having a major impact on phytoplankton phenology and also on the net primary production. Reducing the production significantly reduces the POC (detritus) fluxes about 2 months after the bloom and has significant impact on the trophic efficiency (note that the trophic efficiency in the free run in winter was as high as 4, due to very small phytoplankton concentrations seen by ERSEM in the winter). The reduced POC may impact remineralization in the bottom layer, taking up less oxygen, but the impact of assimilation on the bottom oxygen is less pronounced (Fig. 4.3.4). Although total chlorophyll assimilation does not directly correct the community structure, the phytoplankton community structure is still moderately impacted, probably due to DA updating chlorophyll differently in regions with differing phytoplankton communities. Finally, there is only moderate impact of weakly coupled DA on the inorganic carbon/pH.
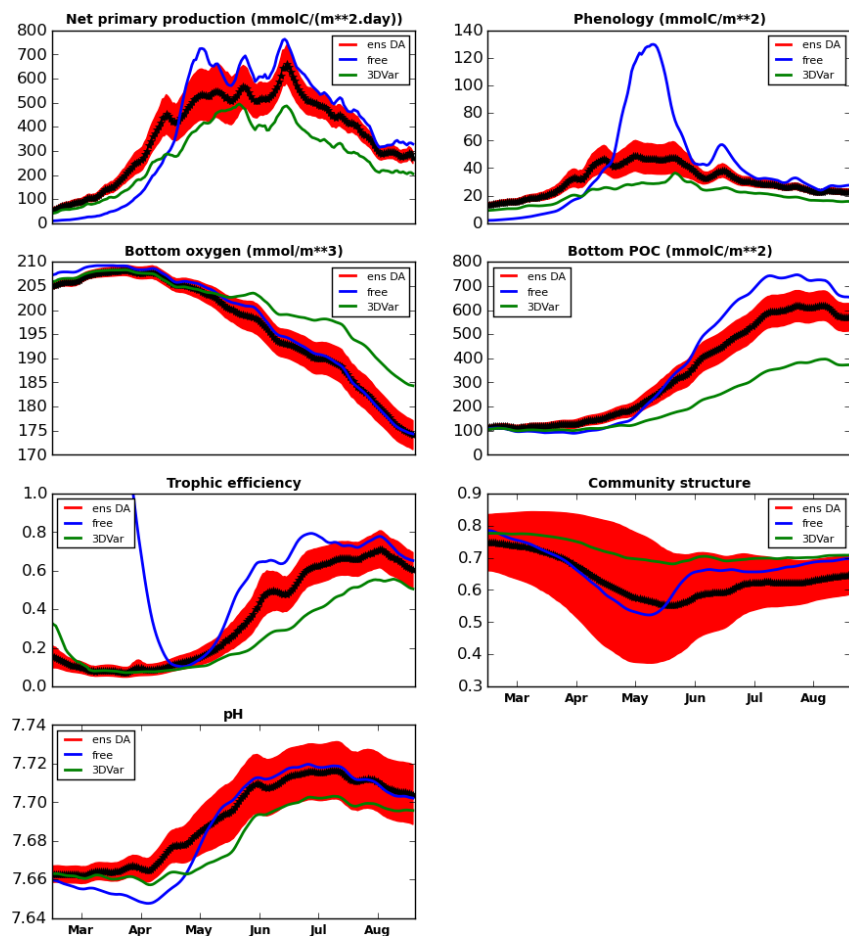
Figure 4.3.4: *The panels compare the SEAMLESS indicators for the ensemble-3DVAr run, the model deterministic free run and the existing 3DVAR system. The plots show the time series for the indicators averaged across the NWE shelf domain (<200m bathymetry). The indicators are defined as in D2.1: (i) net-primary production integrated across the water-column, (ii) phenology is the total phytoplankton carbon integrated across the upper 5 meters of the water column, (iii) bottom oxygen is oxygen concentrations averaged across the bottom 5 meters of the water-column, (iv) POC fluxes is estimated by detritus carbon integrated across the bottom 5 meters of the water column, (v) trophic efficiency is the total zooplankton carbon integrated across the water-column divided by the total phytoplankton carbon integrated across the water-column, (vi) community structure is given as the total diatom and dinoflagellates (macrophytoplankton) chlorophyll integrated across the water-column divided by the total phytoplankton chlorophyll integrated across the water-column and (vii) pH has been averaged across the water-column.*

The validation of the target indicators mostly follows from what has been discussed in the section on observed and non-observed variables. The little available independent validation data suggest that: (1) in terms of phenology, the bloom magnitude and the DCM have been mostly degraded by the weakly coupled DA relative to 3DVAR (e.g Fig. 4.3.5 of report for D3.4), and (2) the weakly coupled ensemble-3DVAR DA run has a similar skill in oxygen than the 3DVAR system (e.g see the discussion in the previous section).

4.4 Assimilation results in the MED MFC domain

To assess the impact of the new balancing scheme that adjusts nutrient profiles based on physical assimilation, one ensemble simulation and three assimilative experiments are carried out using the Mediterranean implementation of the SEAMLESS 1D-prototype described in Deliverable 2.2:

- **ENS**: A 50-member ensemble generated with a set of different initial conditions (standard deviation of physical fields equals to 0.02% and 0.04% for temperature and salinity at surface, respectively) and a set of stochastic meteorological forcings based on ERA5 (standard deviation imposed equal to 20%)

- **EnKF_TS**: An assimilative experiment where T and S profiles from Argo floats are assimilated through an ESTKF scheme and biogeochemistry is indirectly impacted by the dynamical model adjustments. This experiment reflects the current operational MED system.

- **EnKF_TS_VarNut**: An assimilative experiment where T and S profiles are assimilated through an EnKF scheme (ESTKF) and nutrients (phosphate and nitrate) are also updated through the prescribed error covariance scheme described in Section 3.

- **EnKF_TS_Nut:** Ensemble Kalman filter (ESTKF) that assimilates T and S observations, and updates T, S, and nutrient profiles through an evolving error covariance. This experiment allows to assess the difference between a prescribed error covariance based on Argo/BGC-Argo versus an evolving error covariance.

The ensemble and assimilative experiments are carried out on two BGC-Argo floats: 6901772 (green points) and 6902903 (brown points, Fig. 4.4.1) to simulate western and eastern Mediterranean conditions, respectively.
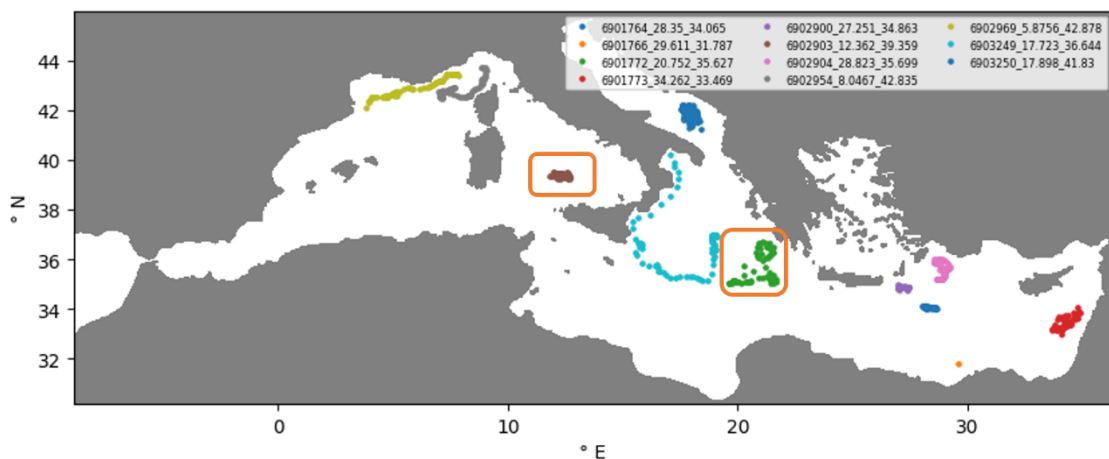

Figure 4.4.1: *Location of 2019 BGC-Argo floats equipped with nitrate sensors. Floats in the orange rectangles have been used in the assimilative experiments: 6902903 and 6901772 BGC-Argo floats in the Tyrrhenian Sea (western Med) and in the Levantine (eastern Med), respectively.*

Diagnostics on observed variables

Temperature and salinity were assimilated in all the ESTKF assimilative experiments producing identical results when considering physical variables since they differ only on the one-way coupling

method that is applied to affect biogeochemical variables. The T and S assimilation show a general reduction of the root mean square differences (RMSDs) between simulations and Argo floats temperature and salinity when compared with ENS (Tab. 4.1.1).

	RMSD float 6901772				RMSD float 6902903			
	Temperature [°C]		Salinity [psu]		Temperature [°C]		Salinity [psu]	
Layers	ENS	EnKF	ENS	EnKF	ENS	EnKF	ENS	EnKF
0-50 m	0.93	0.83	0.54	0.40	0.63	0.64	0.55	0.33
50-100 m	0.85	0.69	0.40	0.34	0.55	0.50	0.45	0.23
100-200 m	0.79	0.52	0.30	0.27	0.50	0.37	0.40	0.27
200-400 m	0.73	0.54	0.28	0.21	0.96	0.93	0.37	0.36
>400 m	0.55	0.47	0.22	0.17	0.73	0.73	0.31	0.31

Table 4.4.1: *Root mean square differences (RMSD) between assimilative experiments and Argo profiles for temperature and salinity.*

Diagnostics on non-observed variables

The assessment of the assimilative experiments on non-observed variables is performed computing root mean square deviations (RMSDs) for nitrate and chlorophyll concentrations using BGC-Argo profiles considering different layers. Results show that the assimilation of T and S with increments limited to T and S (one-way weakly coupled DA, EnKF_TS) provides results very close to the ensemble simulation without assimilation (ENS) considering nitrate, especially in the eastern Mediterranean (float 6901772; Fig. 4.4.2). For float 6902903 in the western Mediterranean (Fig 4.4.3), the differences between ENS and EnKF_TS are noticeable only in the winter (January-March) in the layer 100-200 m.

The use of the prescribed covariance to update nutrients (EnKF_TS_VarNut) impacts the nitrate RMSDs. RMSD reductions with respect to the ENS simulation are observed in the layers 0-50 m, 50-100 m and 100-200 m of both floats from spring to autumn, showing that shape and intensity of nutricline dynamics benefited from the new variational assimilation. In particular, for the eastern float, the RMSD reductions are slightly higher than 10% and 5% from spring to autumn in layer 50-100 m and 100-200 m, respectively. In the 0-50 m layer, the RMSDs of EnKF_TS_VarNut are lower than in ENS by nearly 8% in spring (March-June) and 2% in summer (July-September) on average. Considering the western float, RMSD reductions in the EnKF_TS_VarNut simulation are particularly relevant in spring and summer in the 0-50 m (nearly 20%) and 50-100 m layers (nearly 10%). In the 100-200 m layer, the RMSDs is reduced only in late summer and autumn by nearly 10%. For both float locations, in the deepest layer (200-400 m) the use of the prescribed covariance in EnKF_TS_VarNut slightly increases RMSDs.

Figure 4.4.2: *Nitrate RMSD with respect to float 6901772 (eastern Mediterranean) at four layers (0-50 m, top-left; 50-100 m, top-right; 100-200 m, bottom-left; 200-400 m; bottom-right).*
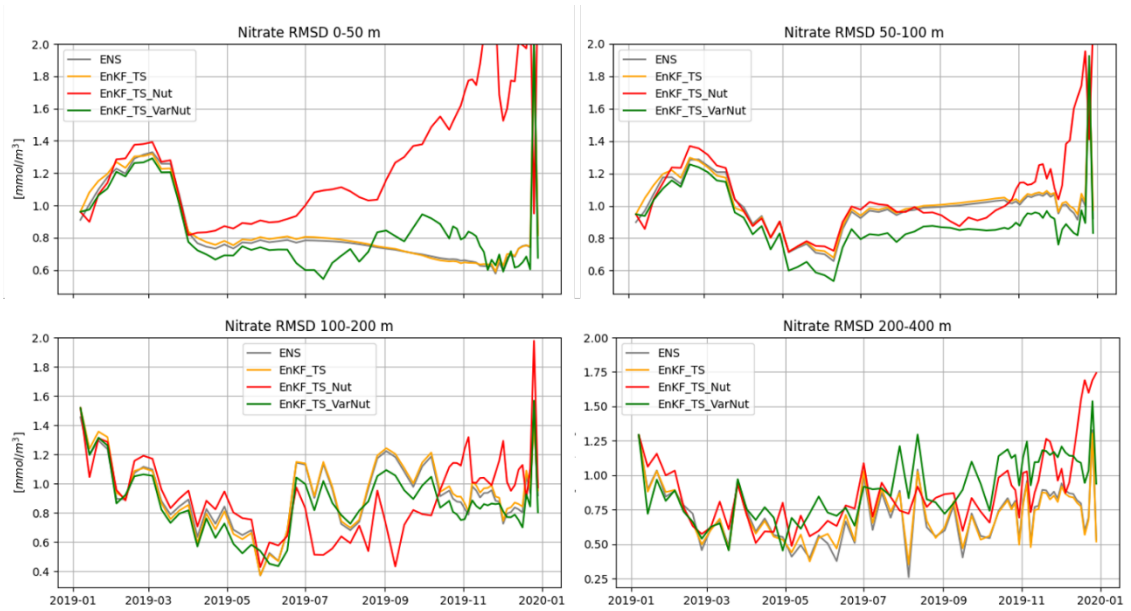

Figure 4.4.3: *Nitrate RMSD with respect to float 6902903 (western Mediterranean) at four layers (0-50 m, top-left; 50-100 m, top-right; 100-200 m, bottom-left; 200-400 m; bottom-right).*

Figure 4.4.4: *Chlorophyll RMSD with respect to float 6901772 (eastern Mediterranean) at four layers (0-50 m, top-left; 50-100 m, top-right; 100-200 m, bottom-left; 200-400 m; bottom-right).*
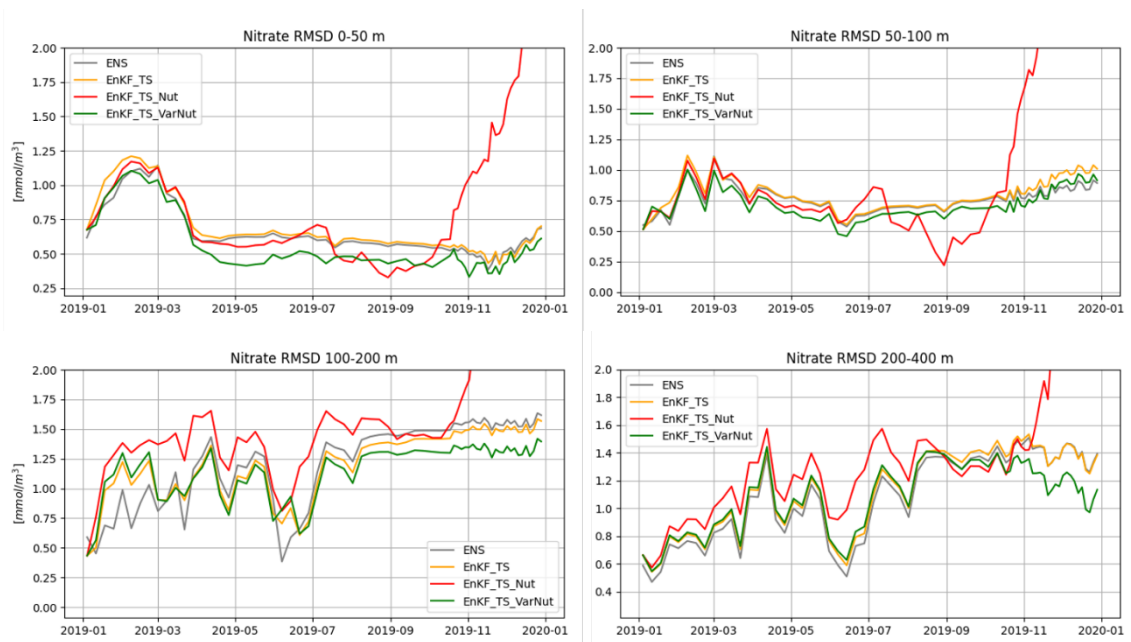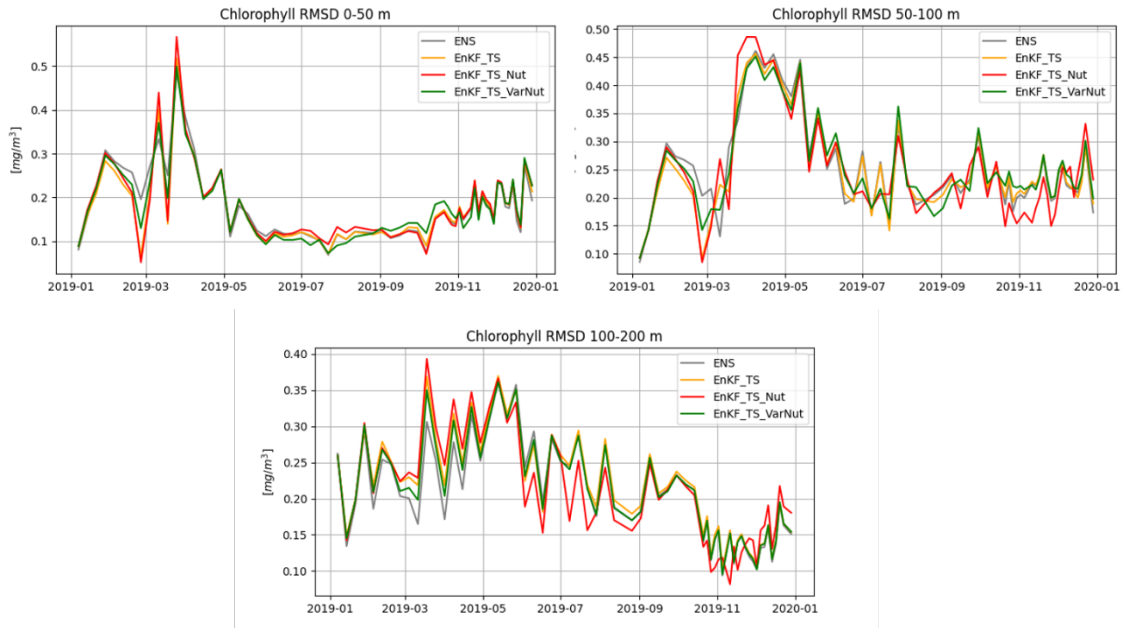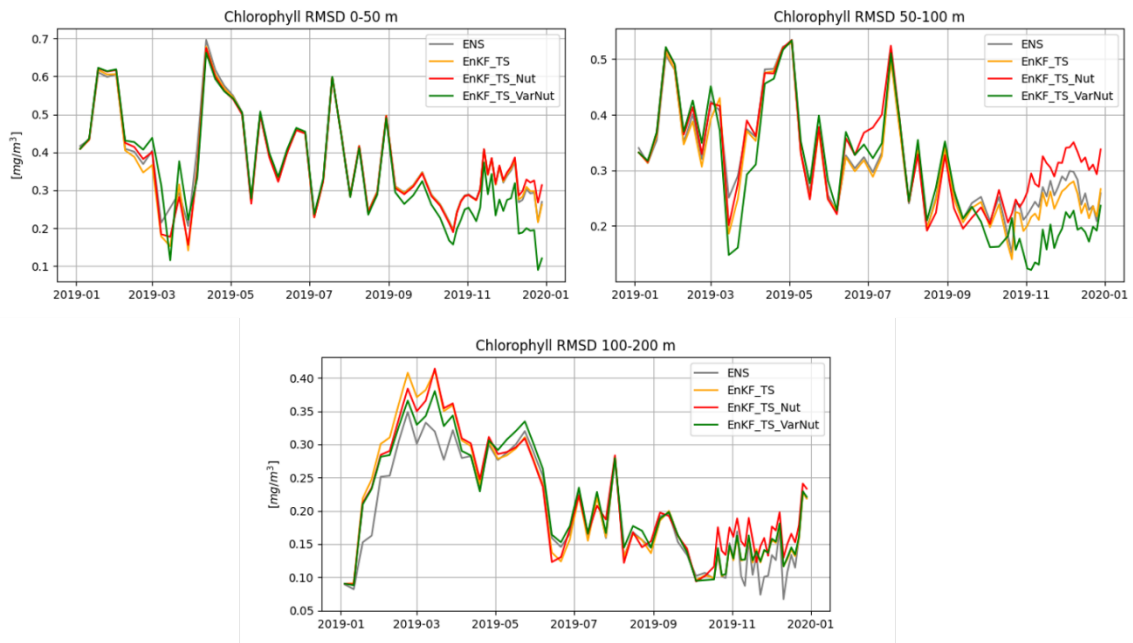

Figure 4.4.5: *Chlorophyll RMSD with respect to float 6902903 (western Mediterranean) at four layers (0-50 m, top-left; 50-100 m, top-right; 100-200 m, bottom-left; 200-400 m; bottom-right).*

The assimilation of T and S with increments on T, S and nutrients through an EnKF approach (EnKF_TS_Nut simulation) produces an increase of nitrate RMSDs with respect to ENS simulation with some exceptions (e.g., eastern float in the 100-200 m layer un summer). Moreover, a relevant degradation on nitrate is evident in autumn for the western float. This case needs further investigation to identify which dynamics produce the degradation that is not detected in eastern case.

The effects of the different assimilation approaches on chlorophyll (Figure 4.4.4 and 4.4.5) are less evident than on nitrate with differences (positive and negative) of the EnKF_TS_VarNut run with respect to ENS simulation close to or lower than 5% for the eastern float. In particular RMSDs reductions of nearly 5% are observed in the 0-50 m layer in winter and spring, while lower reductions occur in the 50-100 m layer (1% to 4%) from winter to summer. Variations of RMSDs for the western float are relatively small with the exception of autumn in the 0-50 m and 50-100 m layer (with RMSD reductions nearly equal to 20%) and a general RMSD increase (nearly 10%) in the 100-200 m layer.

Diagnostics on derived quantities and indicators

The diagnostics on non-observed variables and derived SEAMLESS indicators are provided by the comparison of the ensemble average and standard deviation for integrated 0-200 m primary production, POC at 500 m, biomass of phytoplankton and of zooplankton, and biomass of small and large phytoplankton groups. For each indicator, the seasonal averages of the ENS, EnKF_TS and EnKF_TS_VarNut simulations are compared together with their standard deviations. Metrics are not shown for the EnKF_TS_Nut simulations that are affected by nutrient degradation for western float.

Generally, the impact of the assimilation on indicators is low, whereas the EnKF_TS_VarNut shows larger variations than the only-physics assimilation (EnKF_TS). Seasonal variations of the phytoplankton (Fig. 4.4.6) and zooplankton biomass (Fig. 4.4.7) of the EnKF_TS_VarNut are less than 10% except for autumn in the western float location. The simulations with assimilation show a general reduction of the uncertainty (i.e., decrease of the ensemble standard deviation). The only exception is observed in summer and autumn in the western site for both phytoplankton and zooplankton biomasses.

The ratio of large over total phytoplankton (Figs. 4.4.8 and 4.4.9) shows similar results to those reported for total phytoplankton biomass: seasonal variations of EnKF_TS_VarNut lower than 10% with the exceptions of winter (variations up to 20%) in both sites and in autumn (variation up to 40%) in the western site (not shown). Biomass variations of small and large phytoplankton are generally the same or similar in all seasons and sites, except for the western site in winter, where the assimilation favours the small phytoplankton over the large one. Uncertainty of the EnKF_TS_VarNut decreases in all cases w.r.t. to the reference simulation except for the western site in summer and autumn as already observed for total phytoplankton biomass.

Figure 4.4.6: *Phytoplankton integrated biomass at float locations (top: eastern; bottom: western). Seasonal averages of the ensemble for the ENS, EnKF_TS and EnKF_TS_VarNut simulations (left) and their standard deviation (right).*
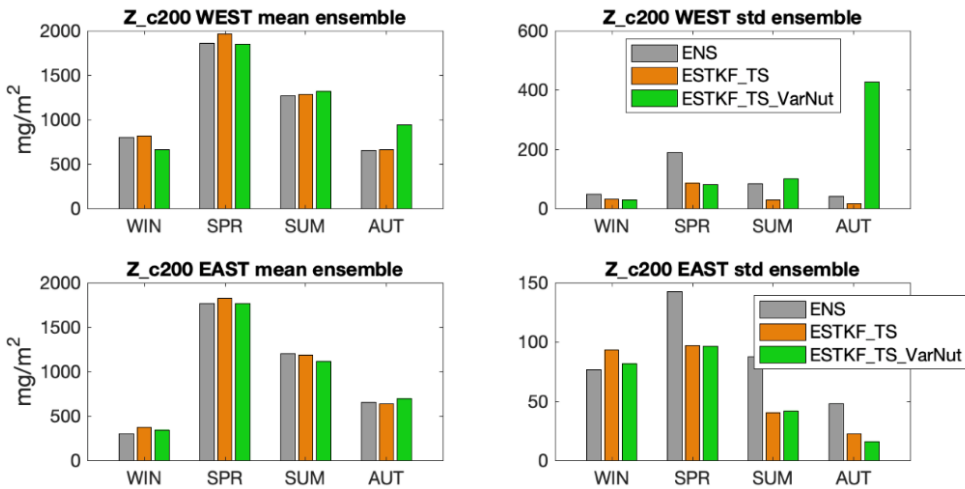
Figure 4.4.7: *Zooplankton integrated biomass at float locations (top: eastern; bottom: western). Seasonal averages of the ensemble for the ENS, EnKF_TS and EnKF_TS_VarNut simulations (left) and their standard deviation (right).*
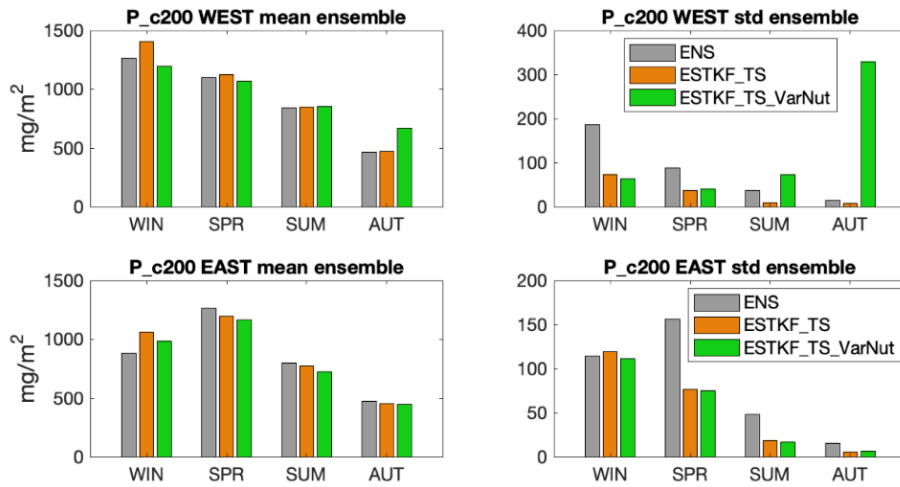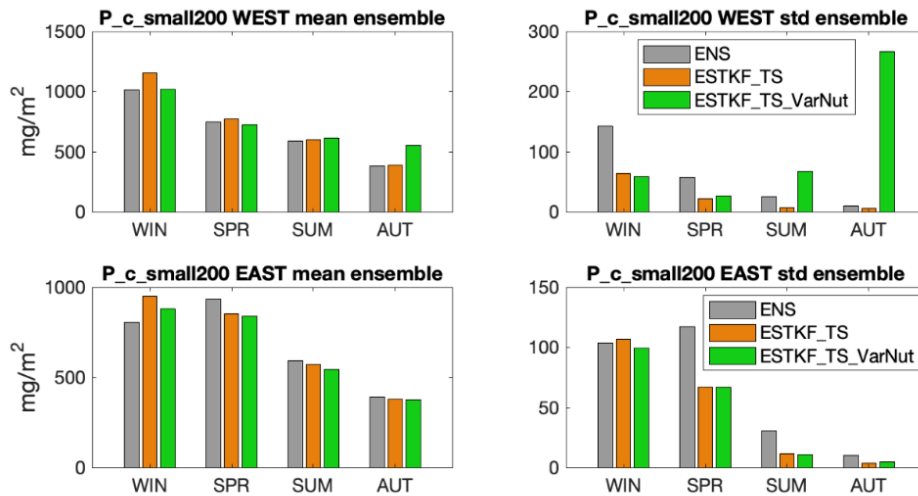
Figure 4.4.8: *Small phytoplankton integrated biomass at float locations (top: eastern; bottom: western). Seasonal averages of the ensemble for the ENS, EnKF_TS and EnKF_TS_VarNut simulations (left) and their standard deviation (right).*
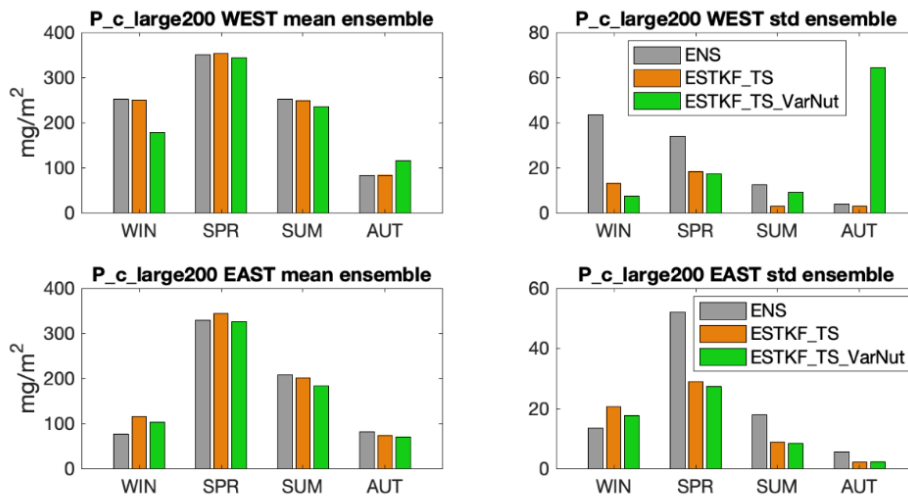
Figure 4.4.9: *Large phytoplankton biomass at float locations (top: eastern; bottom: western). Seasonal averages of the ensemble for the ENS, EnKF_TS and EnKF_TS_VarNut simulations (left) and their standard deviation (right).*

The net primary production (Fig. 4.4.10) of the EnKF_TS_VarNut simulation shows larger variation in the western site compared to the eastern site. In the western site, variations are larger than 15% in all seasons except spring, while variations are always lower than 10% in the eastern site. The uncertainty of the assimilation simulation of net primary production generally decreases with respect to the ENS simulation but it increases in summer in the western site and in autumn in both sites.
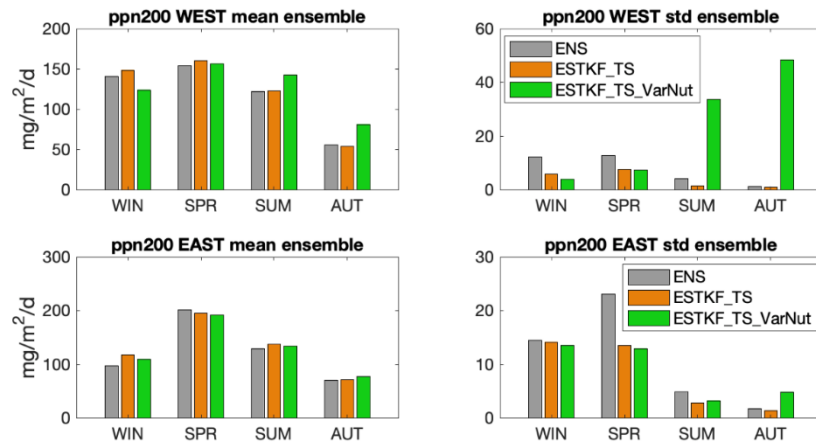
Figure 4.4.10: *Vertically integrated primary production at float locations (top: eastern; bottom: western). Seasonal averages of the ensemble for the ENS, EnKF_TS and EnKF_TS_VarNut simulations (left) and their standard deviation (right).*

Considering the flux of the sink of organic export at 500 m (Fig. 4.4.11), larger absolute variations (i.e., larger than 0.01 mg/m^2/d) of the EnKF_TS_VarNut w.r.t. the reference ENS simulation are registered in spring and summer in both float sites, with the largest variation (up to 400%) in spring in the eastern site. However, this variation is associated with a large increase of the uncertainty (Fig. 4.4.11 bottom right). Beside this case, the uncertainty decreases for both locations in all seasons

Figure 4.4.11: *POC export at 500m at float locations (top: eastern; bottom: western). Seasonal averages of the ensemble for the ENS, EnKF_TS and EnKF_TS_VarNut simulations (left) and their standard deviation (right).*
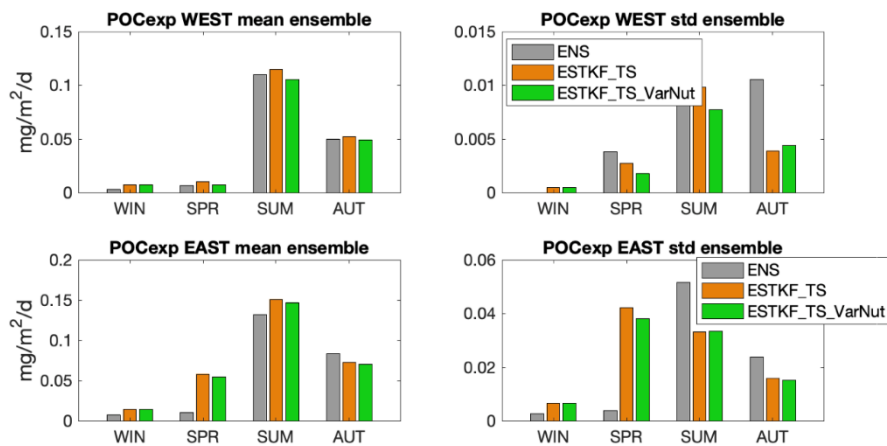
5. Analysis of cost-benefits of weakly coupled DA

In this section we analyse and discuss the benefits of the new developments for weakly coupled DA with regard to the biogeochemistry. The analysis will focus on (Section 5.1) cost-effectiveness as well as (Section 5.2) the benefits regarding the assimilation effects on the indicators.

5.1 Cost Benefits

In general, one has to notice that ensemble-based data assimilation methods have a higher computational cost than using a 3D-Var with parameterized covariances. This is due to the cost of integrating the ensemble of model states, either for generating the prior ensemble of the 4D assimilation scheme tested in the GLO/IBI regions or on-flight during the assimilation process as used in the ensemble Kalman filters applied in the BAL or ARC regions or the ensemble 3D-Var used in the NWS. The higher cost can limit the applicability of the data assimilation scheme for time-critical operational applications, like the processing chain for near-real-time data.

Since the partners in SEAMLESS use different assimilation schemes adapted to the difference MFCs domains, we list the cost considerations separately:

- BAL: Considering that an ensemble of the coupled model has to be run in any case, the additional cost of weakly coupled DA is that the computing time for the assimilation step increases by a factor of about two. This is due to the fact that the physical observations and chlorophyll observations have to be assimilated one after the other. However, this additional execution time is negligible compared to the integration time of the model. In the experiment performed here, the 24-hour forecast took 2200 seconds on average. For comparison the analysis step too 11 seconds if only one of the observation types was assimilated, but 20 seconds for assimilating both sea surface temperature and chlorophyll observations. The comparison is different when one considers that the BAL MFC currently uses an ensemble optimal interpolation scheme. In this EnOI only a single model state is integrated (compared to 30 in the experiments performed here) and ensemble perturbations are generated from output files of a previous model run (similar to the method used in the GLO/IBI experiment but in 3 dimensions with different ensemble perturbations over time). In this case, the required compute resources increase by a factor of 30 when switching to the dynamic ensemble integration used here. At least for the reanalysis product of the BAL-MFC this cost would be too high for operational use given the compute resources that the BAL-MFC can use. On the other hand, the actual execution time would only increase by a few per cent since the ensemble integrations are fully parallelized and only lead to a small overhead in computing time.
- GLO/IBI: The CPU (and data storage) required to perform weakly coupled 4D inversions in 2 steps is doubled when compared to 1-step inversions. However, this extra CPU cost remains negligible when compared to the prior ensemble production, especially in the global domain. The numerical cost of the 2-step updates is therefore not an obstacle for importing the weakly coupled 4D inversion method into an operational system.

- NWS: Running a 30-member ensemble for the NWS increases the simulation cost 2-3 times when compared to the 3DVAR, due to ensemble simulations and extra processing steps to calculate the flow-dependent background covariance matrix from the ensemble. The system needs to be further optimized to be used in near-real time operational applications, but it can still be used for reanalyses.

- MED: Using a hybrid approach to update nutrients based on density increments mainly impacts the amount of data exchanged between the physical and biogeochemical models that run separately. In addition to the usual forcing fields provided by the ocean dynamic model (e.g., u, v, w, eddy diffusivity, T, and S), increments on T and S produced by the physical assimilation should be included. The addition of two variables to the exchanged forcing fields is sustainable in the NRT system at its present state.

5.2 Surface Chlorophyll, phenology

The **Phytoplankton phenology** concerns the timing, amplitude and duration of major blooms. Following Deliverable 2.1 one can in particular consider the value of the maximum of chlorophyll concentration in the layer 0-5m (mgChl m^{-3}), the depth of the maximum of chlorophyll during the summer period (m) and the timing of the bloom, i.e. the time of the year when the two maxima occur (day).

Regarding phenology, the experiments in the different regions show that a significant impact is obtained when chlorophyll observations are assimilated. For the BAL, the assimilation reduced the amplitude of the bloom and lead to a slightly shorter duration of the peak bloom phase. For the GLO/IBI region, the assimilation of surface data produced a much more intense spring bloom, with a peak occurring ~ April 18th and a maximum value that coincided with the L4 data collocated at PAP station (Figure 4.2.4). Further, the assimilation slightly strengthened the sub-surface chlorophyll maximum towards the end of the hindcast period (Figure 4.2.7). For the NWS, it was found that the ensemble-3DVar had a slightly lesser impact on the phenology than the original 3DVar system with parameterized covariances. The weakly-coupled system has also a major impact on deep chlorophyll maxima, which is difficult to validate given a lack of independent data. For the MED the phenology was not directly evaluated, and chlorophyll data was not assimilated. However, the effects observed on the chlorophyll variables show that the assimilation of T and S affects the intensity and timing of the phytoplankton bloom in a limited way.

5.3 Primary Production

The **primary production** is the synthesis of organic compounds from dissolved carbon dioxide through photosynthesis as source of energy. Primary production is computed as the vertical integral of the 0-200m layer.

For primary production the assimilation experiments in the different regions result in a mixed impact. For the BAL region the assimilation of chlorophyll observation resulted in a longer duration of increased primary production. For the GLO/IBI and MED regions, the assimilation impact on primary production, averaged over 2019, is fairly low, with however a change in the seasonality. A peak of vertically integrated primary production is observed during the first weeks of April, anticipating the

surface signature of the spring bloom. For the NWS, the net primary production was substantially impacted by the chlorophyll assimilation, in line with the simulated chlorophyll. This effect was caused by the direct modification of the chlorophyll and carbon variables of the phytoplankton functional types by the chlorophyll assimilation scheme.

5.4 Phytoplankton functional types

The **Phytoplankton Functional Types** (PFT) indicator is computed as the ratio between large phytoplankton biomass and total phytoplankton biomass.

PFTs are analysed in the BAL, NEW and MED regions. The impact of the weakly-coupled assimilations was small to high. For the BAL region, the PFT ratio was decreased due to lower concentrations of diatoms and, partly, an increase of the concentration of flagellates. In the NWS a medium-level impact was obtained since the updates of the PFTs from total chlorophyll are based on model community structure. For the MED region, the influence of the assimilation was small and the dominant group was not changed. The uncertainty was increased by the assimilation in the western Mediterranean site during summer and autumn.

5.5 Particulate Organic Carbon (POC) flux

The **Particulate Organic Carbon (POC)** is defined here as the non-living carbon fraction of particulate organic matter, i.e. the detritus, and is computed as the average concentration of the 0- 200m layer from the model output, or 0-bottom in shallower areas. Here we consider the POC flux, i. e. the sinking flux at a depth of 500m.

The assimilation experiments in all regions, except BAL where POC was not analyzed because of the shallowness of the station Arkona, demonstrate an effect on the POC flux. For the GLO/IBI domain, the POC flux estimates benefit from the use of the one-way weakly coupled assimilation of physical data, while the impact of OC data assimilation largely dominates the effect of altimeter data in the PAP region. In other regions where the co-variability between SSH and OC is stronger, one can expect that the joint assimilation of both products will be more impactful. For the NWS the concentrations of detritus (non-living POC) show a quite significant impact of the chlorophyll assimilation. For the MED region, the additional update of the nutrients generally decreases POC flux uncertainty (ensemble spread). However, in the easter Mediterranean site the uncertainty increased during spring which related to a significant increase of the POC downward flux.

5.6 Trophic efficiency

The **trophic efficiency** is the ratio of production at one trophic level to production at the next lower trophic level. It is computed as the ratio between the zooplankton biomass and the phytoplankton biomass integrated from 0 to 200m depth.

The weakly coupled assimilation induces some changes to the trophic efficiency in the different regions. For the GLO/IBI region the assimilation slightly reduced the TE in the second half of the hindcast period. Further the ensemble spread is reduced. Further investigations for the GLO/IBI region are needed to understand the effects during the forecast period. For the NWS the chlorophyll

assimilation had a major impact both on phytoplankton carbon (direct) and total zooplankton carbon, directly influencing their ratios and hence the TE. For the MED region it was found that the effects on the TE are more relevant in the western Mediterranean site, but the effects are also non-uniform in seasons.

Indicator	ARC	BAL	NWS	IBI/GLO	MED
Phenology	-	Changes	Moderate degradation (glider data)	Moderate improvement (Chl from OC)	Moderate improvement (Chl from BGC-Argo)
PP	-	Changes	N/A	Changes	Improvement (Chl and NO3 from BGC-Argo)
POC flux	-	-	N/A	Changes	Changes
PFT	-	Changes	Changes	N/A	Changes
Trophic efficiency	-	Changes	Changes	Changes	Changes
pH	-	Changes	N/A	N/A	N/A
O	-	Small improvement	Changes	N/A	N/A

Table 5.1. *Summary of effects of the weakly coupled data assimilation in the CMEMS regions. In parenthesis the data is indicated which is used for the assessment. The ARC region is not part of the assessment on weakly coupled assimilation.*

6. Discussion and conclusions

The weakly coupled data assimilation methods assessed here are either ensemble methods with dynamic ensembles, hybrids of an ensemble Kalman filter with a 3D-Var scheme, or hybrid 3D-Var methods that combine an ensemble with parameterized covariances usually based on balance relationships.

Some experiments show a limited influence of the weakly coupled assimilation of physical data onto the biogeochemical variables and SEAMLESS indicators. Thus, the magnitude of the corrections to the physical state of the model is too small to induce a large effect on the biogeochemical variables. This could either be a natural fact in some areas where the biogeochemistry depends less on the physics or a data assimilation setup issue (a too small spread of the ensemble can have the same effect). In the case of the GLO/IBI MFC, the analysis ensemble is over-dispersive, so the area of interest may be less controlled by physics than the other.

For the BAL MFC region a positive effect of the combined weakly coupled assimilation of SST and chlorophyll observations was observed. In the combined assimilation the effect of the physical observations on the biogeochemical fields was larger compared to the case when only physical observations were assimilated. This result is not intuitive because the assimilation of biogeochemical data reduces the ensemble spread and should in principle limit the effect of physical data assimilation on the biogeochemical state but in practice, the assimilation of chlorophyll data may also have set the biogeochemical model in a state that is more sensitive to physical data (to temperature in the case of the BAL MFC).

A positive feature of the 4D scheme implemented in the GLO/IBI region is the smooth temporal evolution of the ensemble members. The temporal evolution is computed dynamically using the NEMO-PISCES model to generate the prior ensemble, while it is computed statistically using the LETKF analysis scheme to generate the posterior ensemble. In this way we avoid dynamical model re-initialization issues which materialize as spurious adjustments of the state variables when the model is highly sensitive to unbalanced initial conditions (Berline et al., 2006; Waters et al., 2017; Park et al., 2018). As a result, in spite of its sub-optimal nature, our 4D approach preserves the smooth temporal evolution of the posterior ensemble when SSH and ocean colour data are assimilated using the 2-step scheme. As a result, the effect of weakly coupled SSH / OC data assimilation is shown to be incremental (see Figure 4.2.4) resulting in reduced uncertainties and modified seasonality of ecological indicators. While the impact of OC data strongly dominates the effect of SSH data assimilation in the PAP region, additional implementations in regions where the co-variability between altimetry and ocean colour is stronger would be worth further R&D investigations.

In the MED region, updating nutrients through a prescribed covariance relationship had a positive influence, while using the dynamic ensemble led to deterioration of nitrate in one of the two investigated locations. The impacts on indicator using prescribed covariance were comparable to those of weakly coupled DA or larger (e.g. primary production).

The different experiments point to further open questions. The ensemble method used in the Baltic Sea shows slightly improved estimates for the ecosystem. However, and open question is the optimal utilization of the covariances between the physics and ecosystem variables. To this end it is unclear which variable transformations, in particular for the ecosystem, would be useful. This aspect should be further investigated.

For the hybrid 3D-Var method used for the NW Shelf the negative impact of the physical DA on chlorophyll needs to be further assessed. At the current stage, the weakly coupled hybrid DA cannot benefit from the combination of physical and biogeochemical observations. When using variational methods, based on the present results we would recommend assimilating the physical data using the 3D-Var with parameterized covariances and combine that with the newly developed (hybrid) ensemble-3D-Var assimilation of chlorophyll. For the hybrid 3D-Var method studied for the Mediterranean Sea using prescribed covariances for the update of nutrients resulted in better DA impact than using the dynamic ensemble information. Here, the reasons for the limitation of the dynamic ensemble are still unknown. In some cases, the uncertainty represented by the ensemble spread increased significantly. This indicated a suboptimal DA process and should be further investigated. For the 4D-method applied for the GLO/IBI MFC domain, the initial results are promising. However, the method needs to be further investigated to assess the influence of the 4D covariances, which are estimated statistically without further model integrations. Recommendations resulting from the experiments discussed above are the following:

- Both physical and biogeochemical observations should be assimilated.
- If possible, it is recommended to assimilate chlorophyll observations that represent phytoplankton functional types corresponding to the model structure
- The distribution of ensembles should be checked for consistency, e. g. by means of rank histograms, using independent verification data.

- Some of the systems experienced difficulties with multivariate data assimilation, which could have several possible causes: perturbation methods, transfer of biases or non-Gaussian variables in the forecast ensemble. Detailed examination of ensemble scatterplots could indicate which settings of the data assimilation can avoid such pitfalls.

Note that the recommendations on weakly coupled assimilation provided in this document should be considered as preliminary and "rules of best practices". These could be adjusted when the results of Task 4.2 on strongly coupled data assimilation will be available. Such changes will be documented in Deliverable 4.2.

7. References

Berline L., Brankart J.M., Brasseur P., Ourmières Y. and Verron J. (2006). Improving the dynamics of a coupled physical-biogeochemical model of the North Atlantic basin through data assimilation: impact on biological tracers, J. Mar. Syst., 64, 153-172, https://doi:10.1016/j.marsys.2006.03.007.

Feudale L., Cossarini G., Bolzon G., Lazzari P., Solidoro S., Teruzzi A., Terzic E., Salon S. Entering in the BGC-Argo era: improvements of the Mediterranean Sea biogeochemical operational system. 9th EuroGOOS International conference, Shom; Ifremer; EuroGOOS AISBL, May 2021, Brest, France. pp.21-29. ffhal-03287500v3, https://hal.archives-ouvertes.fr/hal-03287500v3/document.

Gasparin F., Cravatte S., Greiner E., Perruche C., Hamon M., Van Gennip S. and Lellouche J.-M. (2021). Excessive productivity and heat content in tropical Pacific analyses: Disentangling the effects of in situ and altimetry assimilation, Ocean Modelling, 160, https://doi.org/10.1016/j.ocemod.2021.101768.

Nerger, L., Hiller, W. (2013). Software for Ensemble-based Data Assimilation Systems - Implementation Strategies and Scalability. Computers and Geosciences, 55, 110-118. doi:10.1016/j.cageo.2012.03.026

Park, J.-Y., Stock, C. A., Yang, X., Dunne, J. P., Rosati, A., John, J., et al. (2018). Modeling global ocean biogeochemistry with physical data assimilation: A pragmatic solution to the equatorial instability. *Journal of Advances in Modeling Earth Systems*, 10, 891- 906, https://doi.org/10.1002/2017MS001223.

Pham, D.T., Verron, J., Roubaud, M.C. (1998). A singular evolutive extended Kalman filter for data assimilation in oceanography. Journal of Marine Systems 16, 323–340. https://doi.org/10.1016/S0924-7963(97)00109-7.

Salon, S., Cossarini, G., Bolzon, G., Feudale, L., Lazzari, P., Teruzzi, A., Solidoro, C., Crise, A. (2019). Novel metrics based on Biogeochemical Argo data to improve the model uncertainty evaluation of the CMEMS Mediterranean marine ecosystem forecasts. Ocean Science 15, 997–1022. https://doi.org/10.5194/os-15-997-2019.

Skakala, J., Bruggeman, J., Brewin, R. J., Ford, D. A., & Ciavatta, S. (2020). Improved representation of underwater light field and its impact on ecosystem dynamics: A study in the North Sea. *Journal of Geophysical Research: Oceans*, *125*(7), e2020JC016122.

Project	SEAMLESS No 101004032	Deliverable	D4.1
Dissemination	Public	Type	Report
Date	21 July 2023	Version	4.0

Skákala, J., Ford, D., Bruggeman, J., Hull, T., Kaiser, J., King, R.R., Loveday, B., Palmer, M.R., Smyth, T., Williams, C.A. and Ciavatta, S. (2021). Towards a multi-platform assimilative system for North Sea biogeochemistry. *Journal of Geophysical Research: Oceans*, *126*(4), p.e2020JC016649.

Skákala J, Bruggeman J, Ford D, Wakelin S, Akpınar A, Hull T, Kaiser J, Loveday BR, O'Dea E, Williams CA, Ciavatta S. (2022). The impact of ocean biogeochemistry on physics and its consequences for modelling shelf seas. *Ocean Modelling*. 172:101976.

Dobricic Srdjan, and Nadia Pinardi (2008). An oceanographic three-dimensional variational data ssimilation scheme. Ocean Modelling, 22 (3-4) 89-105.

Storto, A., Masina, S., Navarra, A., (2015). Evaluation of the CMCC eddy-permitting global ocean physical reanalysis system (C-GLORS, 1982-2012) and its assimilation components. Quarterly Journal of the Royal Meteorological Society, 142, 738–758, doi: 10.1002/qj.2673.

Teruzzi, A., Bolzon, G., Feudale, L., Salon, S., Cossarini, G. (2021). Deep chlorophyll maximum and nutricline in the Mediterranean Sea: emerging properties from a multi-platform assimilated biogeochemical model experiment. Biogeosciences, 18(23), 6147-6166.

Waters, J., Bell, M. J., Martin, M. J., & Lea, D. J. (2017). Reducing ocean model imbalances in the equatorial region caused by data assimilation. Quarterly Journal of the Royal Meteorological Society, 143(702), 195–208.